Lanza et al. *Swiss Journal of Geosciences* (2022) 115:2
https://doi.org/10.1186/s00015-021-00400-x

SGG SGS sc | nat
Swiss Journal of Geosciences

ORIGINAL PAPER Open Access

The Saint-Ursanne earthquakes of 2000 revisited: evidence for active shallow thrust-faulting in the Jura fold-and-thrust belt

Federica Lanza[1*], Tobias Diehl[1], Nicholas Deichmann[1], Toni Kraft[1], Christophe Nussbaum[2], Senecio Schefer[2] and Stefan Wiemer[1]

Abstract

The interpretation of seismotectonic processes within the uppermost few kilometers of the Earth's crust has proven challenging due to the often significant uncertainties in hypocenter locations and focal mechanisms of shallow seismicity. Here, we revisit the shallow seismic sequence of Saint-Ursanne of March and April 2000 and apply advanced seismological analyses to reduce these uncertainties. The sequence, consisting of five earthquakes of which the largest one reached a local magnitude (M_L) of 3.2, occurred in the vicinity of two critical sites, the Mont Terri rock laboratory and Haute-Sorne, which is currently evaluated as a possible site for the development of a deep geothermal project. Template matching analysis for the period 2000–2021, including data from mini arrays installed in the region since 2014, suggests that the source of the 2000 sequence has not been persistently active ever since. Forward modelling of synthetic waveforms points to a very shallow source, between 0 and 1 km depth, and the focal mechanism analysis indicates a low-angle, NNW-dipping, thrust mechanism. These results combined with geological data suggest that the sequence is likely related to a backthrust fault located within the sedimentary cover and shed new light on the hosting lithology and source kinematics of the Saint-Ursanne sequence. Together with two other more recent shallow thrust faulting earthquakes near Grenchen and Neuchâtel in the north-central portion of the Jura fold-and-thrust belt (FTB), these new findings provide new insights into the present-day seismotectonic processes of the Jura FTB of northern Switzerland and suggest that the Jura FTB is still undergoing seismically active contraction at rates likely < 0.5 mm/yr. The shallow focal depths provide indications that this low-rate contraction in the NE portion of the Jura FTB is at least partly accommodated within the sedimentary cover and possibly decoupled from the basement.

Keywords: Shallow seismicity, Jura fold-and-thrust belt, Focal mechanisms, Synthetic forward modelling, Seismotectonics

1 Introduction

A region where neotectonic activity is a subject of controversies among earth scientists to this date is the Jura fold-and-thrust belt (FTB), north of the Western Alps. To explain the Jura FTB's genesis, most authors advocate tectonic models of thin-skinned compression which postulate a complete decoupling between basement and cover along a basal decollement horizon formed by the mechanically weak Middle and Upper Triassic evaporites. In this model, the compression is due to the distant push of the emplacement of the External Crystalline Massifs (Fernschub hypothesis: Burkhard, 1990; Buxtorf, 1907; Jordan, 1992; Laubscher, 1961; Müller & Briegel, 1980; Sommaruga & Burkhard, 1997; Sommaruga et al., 2017). Others, on the contrary, support a thick-skinned deformation at the origin of the main structural features

Editorial handling: György Hetneyi.

*Correspondence: federica.lanza@sed.ethz.ch
[1] Swiss Seismological Service, Swiss Federal Institute of Technology, ETH Zürich, Sonneggstrasse 5, 8092 Zürich, Switzerland
Full list of author information is available at the end of the article

within the Jura FTB, where pre-existing basement faults play an active role (Pavoni, 1961; Pfiffner et al., 1997). Recently, there has been some consensus over the thick-skinned vs. thin-skinned controversy, by which the thin-skinned origin can be reconciled with a thick-skinned reactivation of basement structures in the latest Pliocene, i.e., during a late stage or after the formation of the thin-skin Jura FTB (Becker, 2000; Giamboni, Ustaszewski, et al., 2004; Giamboni, Wetzel, et al., 2004; Madritsch et al., 2008; Ustaszewski & Schmid, 2006, 2007; Ustaszewski et al., 2005a). However, contrasting opinions and controversies between currently ongoing compression, transpression or even arc-parallel extension still dominate the literature. There is no agreement on whether the deformation in the northwestern Alpine foreland still predominantly affects the sedimentary cover (decoupled deformation, ongoing thin-skinned tectonics) or whether basement and cover are coupled and deform by the same amount (coupled deformation, thick-skinned tectonics). Ziegler and Fraefel (2009), for example, have reconstructed the Neogene evolution of the drainage systems in the northeastern portion of the Jura FTB and Upper Rhine Graben and concluded that the modern river patterns reflect a response to thick-skinned deformation of the Jura FTB. In a study based on (re)interpreted 2-D reflection seismic data and geological 3-D modeling, Mock and Herwegh (2017) also suggest a change from late Miocene thin-skinned to Pliocene to present-day incipient thick-skinned tectonics. Answers to such questions can be found from the analysis of shallow seismicity, such as the determination of absolute depths and source properties (i.e., focal mechanisms), which, although it is challenging, can provide valuable constraints for the interpretation of seismotectonic regimes in the upper crust of the northern Alpine foreland (e.g., the Fribourg Fault zone, Kastrup et al., 2007; Vouillamoz et al., 2017). In turn, the reconstruction of seismic strain and seismogenic stress regimes in the crust is of critical importance for the assessment of seismic hazard, including risk mitigation strategies regarding potential induced seismicity in the context of geothermal projects or underground nuclear waste repositories. In particular, in the area of interest of northeastern Switzerland, two critical sites are present: (1) the Mont Terri underground rock laboratory, a unique platform to study the performance of a geological repository (Thury & Bossart, 1999); and (2) the Haute-Sorne site where planning for a deep geothermal project is currently under consideration.

In this study, we focus on the seismological re-analysis of the shallow seismic sequence of Saint-Ursanne of the year 2000, located within 5 km from the Mont Terri Lab and Haute-Sorne site, and document challenges posed by its very shallow focal depth. We present (1) a quality assessment of all the earthquake catalogues available to date in the region with the objective to separate natural seismicity from man-made quarry blasts, very common in the area of investigation; (2) template matching analysis of the Saint-Ursanne seismic sequence of 2000 to better define the activity rate as well as its possible mechanical behavior (e.g., presence of repeaters, creep); (3) review of absolute locations with focus on focal depths using a new 3-D Pg + Sg relocation approach (Diehl et al., 2021) and employing forward waveform modelling for the largest magnitude event to discriminate between sources located in the sediment covers versus in the pre-mesozoic basement. This analysis provides new seismological testimony of active shallow reverse (thrusting) deformation in the northern portion of the Jura FTB.

1.1 Regional tectonic and geological setting of the northern Jura fold-and-thrust belt

The study area is located in northwestern Switzerland at the junction of the southern end of the Upper Rhine Graben (URG) and the northern Jura FTB (Fig. 1). The Jura FTB formed within a relatively short time span between the Late Miocene and Early Pliocene as a consequence of Alpine subduction and collision. This typical fold-and-thrust belt is one of the best studied orogenic arcs in the world (e.g., Aubert, 1949; Becker, 2000; Burkhard, 1990; Dèzes et al., 2004; Giamboni, Ustaszewski, et al., 2004; Heim, 1919; Henry et al., 1997; Laubscher, 1997, 2010; Lebeau, 1951; Lyon-Caen & Molnar, 1989; Pfiffner, 2017; Rollier, 1903; Schlunegger et al., 1997; Sommaruga, 1999; Sue & Schmid, 2017; Ustaszewski & Schmid, 2006). In the following, we focus mainly on the regional aspects that are key to the understanding of the neotectonic setting for the Saint-Ursanne seismic sequence of 2000. For a more exhaustive description of the regional tectonics and geology we refer to e.g. Sommaruga et al. (2017) or Rabin et al. (2018) and references therein. The tectonics of the study region within the northern boundary of the Jura FTB is affected by at least two inherited basement structures: (1) the Late Palaeozoic ENE- to NE-oriented basement faults from the Variscan orogeny and subsequent (Late Carboniferous to Permian) post-orogenic extension (Laubscher, 1986; Schumacher, 2002; Ziegler, 1992); and (2) the "Rhenish" structures: NNE-SSW to ENE-WSW striking normal faults associated to the Paleogene intracontinental rifting phase that, in this region, correspond to the Upper Rhine Graben (URG; Lacombe et al., 1993, and references therein; Madritsch et al., 2009). During this regional WNW-ESE extension, the sedimentary cover above the re-activated basement faults developed ENE-trending extensional flexures; which define the main strike of the Permo-Carboniferous trough system (Ustaszewski & Schmid, 2006; Ustaszewski et al., 2005).

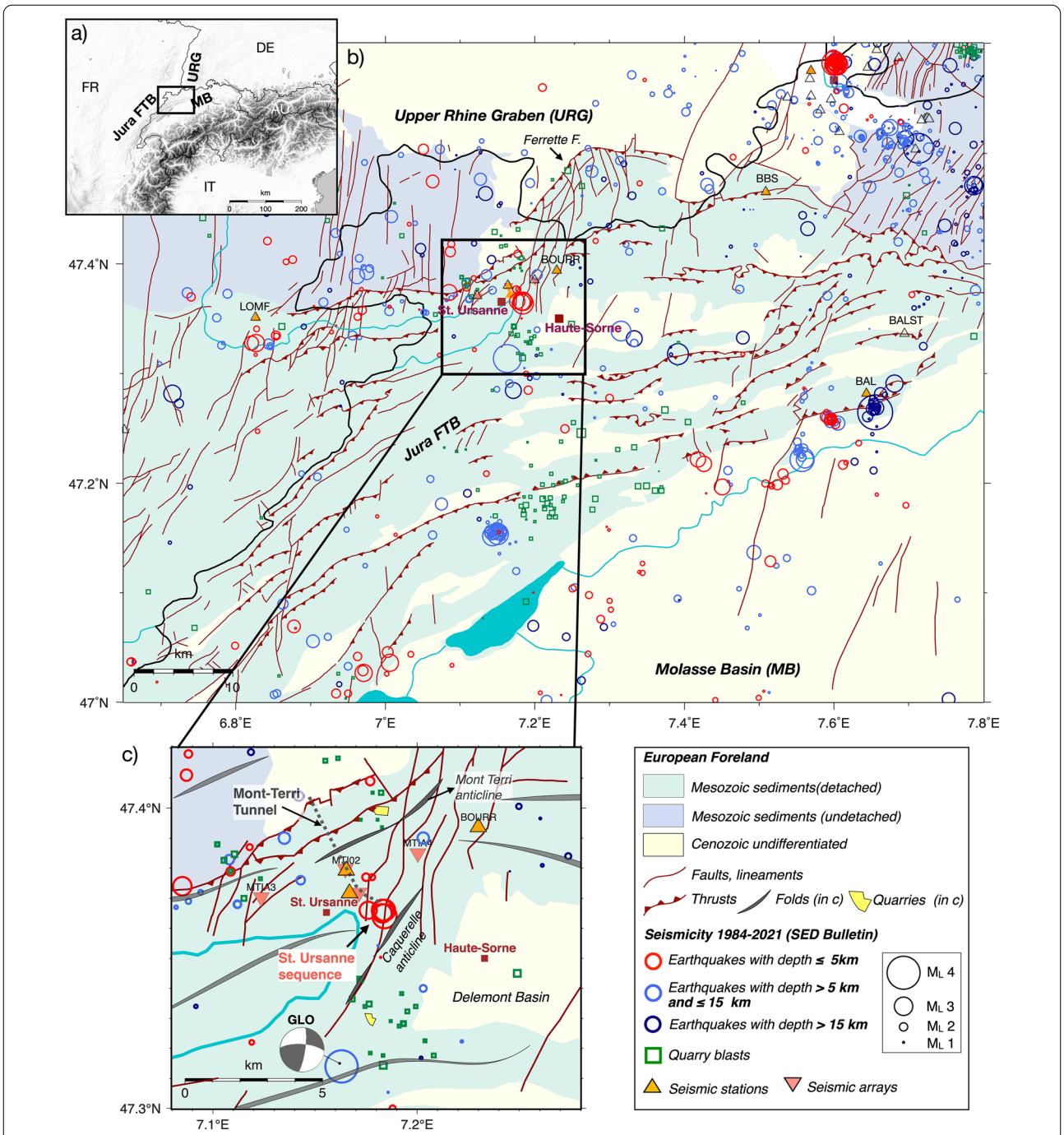

Fig. 1 **a** Location of the study area within Switzerland. The inner inset corresponds to the tectonic map in (**b**). **b** Tectonic map with the main units, fault systems, seismicity and seismic stations in the northern part of the Jura FTB. Faults and fold systems are from swisstopo database (Swisstopo, 2005). Circles indicate earthquakes as listed in the bulletin of the Swiss Seismological Service (SED) between 1984 and 2021 with colors indicating focal depths (see legend). Green squares indicate identified quarry blasts. **c** Zoom in of the area of investigation with the location of the Mont Terri tunnel (dashed line) and the quarries (yellow polygons) indicated

In contrast to the southwestern portion of the Jura FTB, the northern and eastern parts of the folded Jura front are characterized by E-W to NE-SW trending fold axes and thrusts as well as N-S striking left-lateral strike-slip faults. Notably, we find the NNE-oriented Caquerelle anticline that closes the Delemont Basin westwards (Fig. 1b, c).

This orientation confirms the presence of the inherited basement normal faults at depth developed in the Paleogene intra-continental rifting phase (Laubscher, 1963a, 1963b). Focal mechanisms calculated for the M_L 3.7 earthquake that occurred on December 11th, 1987 near Glovelier at a depth of about 9 km indicates a left-lateral strike-slip fault on a steeply E-dipping fault plane (Fig. 1c, Deichmann, 1990), confirming an NNE trending. Further to the north the Ferrette fault (Fig. 1b) has an ENE-orientation before displaying a E-W trends to its eastern end. It is thought that the Ferrette fault has evolved as a result of the superposition of "Rhenish" NNE-trending faults and re-activated ENE-striking Late Paleozoic basement faults (Fig. 1b; Ustaszewski & Schmid, 2007; Ustaszewski et al., 2005), forming a diffuse transfer zone in the north-eastern part of the Mont Terri region.

The Jura FTB consist of Mesozoic and Cenozoic deformed marls and limestones that were detached from both the underlying Paleozoic basement and the undeformed Lower Triassic sandstone series of the Buntsandstein unit, which are considered part of the mechanical basement (Sommaruga et al., 2017). The detachment zone coincides with the Middle Triassic evaporites of the Muschelkalk unit, specifically the Zeglingen Formation according to the Lithostratigraphic Lexicon of Switzerland (www.strati.ch; Affolter & Gratier, 2004). The oldest rocks that outcrop in the region of Saint-Ursanne are the Upper Triassic dolomitic marls, dolomites, and evaporites of the Keuper unit (the Klettgau Formation in the Lithostratigraphic Lexicon of Switzerland) and the immediately younger calcareous, marly, and argillaceous rocks of the Lias group (the Staffelegg Formation in the Lithostratigraphic Lexicon of Switzerland; Reisdorf et al., 2011), the latter hosts a rheologically weak detachment level formed by bituminous shales (Nussbaum et al., 2017). Together, these rocks form the core of the Mont Terri anticline (Fig. 1c; Freivogel & Huggenberger, 2003; Laubscher, 1963a, 1963b). Here, the Lias group is followed by a monotonous succession of Middle Jurassic dark argillaceous rocks belonging to the Dogger Formation (the Opalinus Clay in the Lithostratigraphic Lexicon of Switzerland, Bläsi et al., 1991; Bossart & Thury, 2008; Bossart et al., 2017; Schaeren & Norbert, 1989; Wetzel & Allia, 2003).

2 The earthquake sequence of Saint-Ursanne

In March and April 2000, five earthquakes with a local magnitude for the largest event reaching M_L 3.2 occurred near Saint-Ursanne, in the vicinity of the Mont Terri rock laboratory (Fig. 1b, c); they were widely felt by the population, as reported in Baer et al. (2001). The sequence is dominated by signals with high waveform similarity as well as strong and long-lasting surface wave codas (Fig. 2a). Initial routine location results computed by the Swiss Seismological Service (SED) pointed to focal depths of 6–7 km, corresponding to a source in the Paleozoic crystalline basement (Baer et al., 2001). However, because of the presence of a strong surface wave

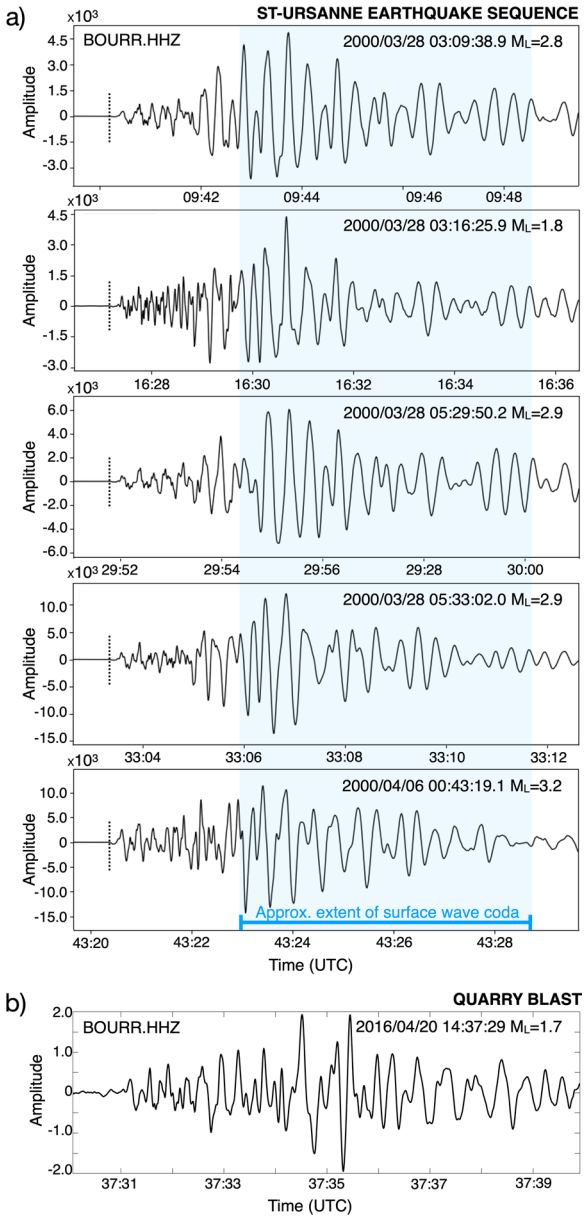

Fig 2 **a** Seismograms of the five earthquakes of the 2000 sequence recorded at station BOURR (epicentral distance ~ 5 km). **b** Seismogram of an identified quarry blast from the SED Bulletin located ~ 3 km north of the earthquake sequence of the year 2000 observed at the same station (epicentral distance 7.8 km). Although both blasts and earthquakes are characterized by a strong surface wave component, waveform similarities are low (cross-correlation values < 0.3)

component, similar to what is usually observed from quarry blasts at the Earth's surface, it is more likely that a rather shallow source, within the Mesozoic sedimentary cover of the Jura FTB, is responsible for the observed signals (Baer et al., 2001). Figure 2b shows a comparison between a quarry blast with SED Bulletin location ~ 3 km north of the sequence of the year 2000. Both blasts and earthquakes are characterized by a strong surface wave component, qualitatively pointing to a first-order location in the sediments rather than in the Paleozoic crystalline basement. On the other hand, this first-glance similarity documents the problem of distinguishing natural seismicity from quarry blasts in the study region. Note that, although they share the surface waves component, the waveform similarities are low (cross-correlation values of < 0.3, see Sect. 3.3).

The routinely determined hypocenter locations of the Saint-Ursanne sequence of the year 2000 published in Baer et al. (2001) are based only on data from stations operated by the Swiss Seismological Service, located in a regional 1-D velocity model. In a first attempt to improve the locations of events that occurred in an area of 14 × 12 km around Saint-Ursanne between 2000 and 2010, waveform recordings from networks in France (Renass) and southern Germany (LED) were merged with the SED data and all arrival times were re-picked in a consistent manner. Corresponding hypocenters were relocated using NonLinLoc, a probabilistic non-linear global-search algorithm of Lomax et al. (2000), in combination with the regional 3-D P-wave velocity model of Husen et al. (2003). Judging from the consistent clustering of events with similar waveforms, the epicentral locations were improved significantly by this procedure (Deichman et al., 2012). However, the remaining uncertainty in focal depth accuracy related to insufficient knowledge of the local seismic velocity structure so far hampered a discrimination between shallow (z < 10 km) and very shallow source locations (z < 5 km).

3 Data

3.1 Seismic stations in operation to date

Taking advantage of the facilities provided by the Mont Terri rock laboratory, the Swiss Geological Survey (swisstopo) initiated a pilot project in 2014 aimed at a detailed characterization of the seismicity of the area surrounding the rock laboratory. For this purpose, an ad-hoc dense seismic network was installed in 2014–2015 and is still operated continuously to date. The network consists of three stations operated by the Swiss Seismological Service (SED) since 2016, two of which are located in tunnels of the rock lab (MTI01, MTI02), whereas the third one is located on the surface above the laboratory (MTI03). Stations MTI01 and MTI03 are accelerometers (EpiSensor ES-T), whereas station MTI02 is a velocity sensor (STS2 3-component broad-band). Additionally, the region hosts four mini-arrays (SNS—seismic navigating systems; Joswig, 2008; Wust-Bloch & Joswig, 2006) with a network extension of about 6 km. Each mini-array consists of a central 3-component short-period seismometer (LE-3Dlite) and three 1-component seismometers (LE-1Dlite), which are deployed within a distance of ~ 100 m from the central station. Two mini-arrays (MTIA1 and MTIA2) are installed within the tunnel system of the laboratory, whereas MTIA3 and MTIA4 are located at the surface about 3 km to the west and to the east of the tunnel system, respectively. All stations are part of the national network since 2016 and available data are stored in the SED archive and are publicly accessible from the SED data portal (http://seismo.ethz.ch/en/research-and-teaching/products-software/http://seismo.ethz.ch/en/research-and-teaching/products-software/http://seismo.ethz.ch/en/research-and-teaching/products-software/). For this study, only the central 3-component sensors were used. In addition to this dense local network, the permanent station BOURR is located ~ 5 km east of Saint-Ursanne and has been recording since 1998 (Additional file 1: Table S1). Several other stations are operated by the SED as well as French and German agencies in the wider study region (Fig. 1, Additional file 1: Table S1).

3.2 Seismic catalogues

3.2.1 SED catalogue (2000–2021)

Since 2000, 44 natural earthquakes are listed in the SED Earthquake bulletin within a radius of 10 km of Saint-Ursanne. In this time period and radius, focal depths range between −0.7 and 21.5 km with magnitudes in the range of $M_L = 0$ to $M_L = 3.2$ (Additional file 1: Table S2). We report here only the events recorded after 2000 because the quality of the locations prior to the year 2000 is very poor and a consistent and uniform analysis of all the events before 2000 would be also hindered by the change of the network from short-period to broad-band between the years 1998 and 2002. The earthquake sequence of the year 2000 stands out as the only temporal and spatial concentration of events. Many quarries are located in the area, and up to the end of 2020, the SED catalogued 25 explosion-type events identified as quarry blasts. Identification of quarry blasts is done manually and is based on waveform inspection (e.g., surface waves content), spatial correlation with a quarry site, and origin time and day (e.g., blasts events usually take place during the week around mid-day). Occasionally, confirmation is also obtained directly from the quarry operators. For an extensive description of the methods and software currently used at the SED for routine earthquake analysis

and catalogue production, we refer to Diehl et al., (2014, 2018).

3.2.2 *Stuttgart and Seismic Solution catalogues (2014–2015 and 2017–2018)*

Starting in 2014, with the installation of the local mini-arrays (SNS), the Institute for Geophysics of the University of Stuttgart (IFG) co-lead together with swisstopo the efforts to map additional potential microseismic activity of local fault systems of the area surrounding the Mont Terri Lab (Blascheck, 2018). They implemented the NanoSeismicSuite software (Joswig, 2008; Sick et al., 2012), an algorithm that aims to detect low energy signals in noisy environment via sonograms. Sonograms are spectrograms with dynamic frequency-dependent noise adaptation that facilitate the detection and characterization of events in low-SNR conditions on single or multiple traces (Joswig, 2008; Sick et al., 2012; Vouillamoz, Kraft, et al., 2016; Vouillamoz, Wust-Bloch, et al., 2016). For the year 2014–2015, they identified ~ 90 additional locatable microseismic events within a radius of 10 km from the Mont Terri rock laboratory (Abednego et al., 2017; Blascheck, 2018). Since July 2017, due to the closing of the IFG, data analysis is performed by the company Seismic Solutions GbR, Tubingen, Germany. They provide annual reports on the characteristics and distribution of the natural seismicity in and around the Mont Terri rock lab using the NanoSeismicSuite software as earthquake detector and locator. The last published catalogue counts 135 events for the period from July 2017 to June 2018, of which 16 were classified as local earthquakes.

3.3 Quality assessment and harmonization of seismic catalogues

Due to the large number of quarry-related activity in the area, a validation of the micro seismicity catalogues provided by Stuttgart and Seismic Solutions is warranted. In order to reliably identify a natural versus an anthropogenic origin for the additional events detected through Nanoseismic monitoring, we conducted a re-evaluation of each event. Of the 90 events during the period of 2014–2015, 64 events (71%) are either too weak (i.e., they have a too low signal-to-noise ratio) to properly determine first arrival times or a source origin, or they show spatial and temporal correlations with quarry sites and blasts. In particular, 25 events (28%) occur during typical blasting times (week days between 6 am to 6 pm), show high cross-correlation (CC) values with signals of known quarry blasts (0.52–0.90) and are located close to active quarries (the estimated absolute epicentral uncertainties for quarry blasts is between 0.5 and 1.5 km in the region). Cross-correlation values were obtained by normalized cross-correlation between template waveforms (e.g., known quarry blasts) and each microseismic event trimmed to 10 s length with 2 s taken before the origin time. Waveforms were filtered between 2 and 30 Hz with a causal 4th order Butterworth filter.

For comparison, we also cross-correlated waveforms of 16 known quarry blasts with the five events of the 2000 Saint-Ursanne earthquake sequence. Except for four isolated cases, for which we obtained a CC value of 0.52, all the other quarry blasts showed weak correlations with the sequence, with CC values less than 0.3. This test demonstrates that, even though the signals of both the earthquake sequence and the quarry blasts share a strong surface wave component, their overall waveform similarity is not significant. As a consequence, only 8 night-time events (~ 9%) were retained for further analyses (see Additional file 1: Table S3, and Sect. 4.1). Of the 135 events during the period 2017–2018, after a manual review, 13 events among the local 16 earthquakes were retained and three events from the "unsure" class of the Seismic Solution 2017–2018 catalogue were added (Additional file 1: Table S4). In summary, of the 225 microseismic events from both the Stuttgart catalogue of 2014–2015 and the Seismic Solution catalogue of 2017–2018, we were able to confidently identify and classify as local earthquakes a total of 24 events.

4 Methods: seismological investigations

4.1 Template matching analysis

The recent densification of the seismic network in the region of interest provides an opportunity to lower the magnitude threshold of the detected earthquakes and gain insights into the long-term evolution of the 2000 Saint-Ursanne sequence. In this study, we use template matching detection techniques based on waveform cross-correlation (similarity) to gain additional information about the sequence. The motivation to use a cross-correlation detector lies in the hypothesis that, if the events of the year 2000 are matched with earthquakes in the period after 2014, additional data recorded by stations within very short epicentral distances will be available to constrain the location, focal depth and the source mechanism of the original sequence. Here we use a multi-template, single station approach using the python-based software *seismatch* (Hermann et al., 2019; https://gitlab.seismo.ethz.ch/microEQ/TM). We run *seismatch* on six separate stations: BOURR, MTI02, MTIA1, MTIA2, MTIA3, MTIA4. The template matching is performed on all three channels (Z, E, N). After assessing the influence of different passbands, waveforms were filtered between 2 and 30 Hz with a causal 4th order Butterworth filter. The chosen width of the passband reduces the number

of false detections without substantially degrading the waveform similarity of closely spaced hypocenters. The duration of all template waveforms was set to 10 s. To declare a detection, we set a minimum cross-correlation value (CC) of 0.40, that had to be exceeded at all components at the same time. The minimum of the CC values was then taken as the similarity measure of a detection to its template. Upon visual inspection of the results, we assigned template-specific cross-correlation thresholds above which we considered the detection to be trusted (Additional file 1: Table S5). The templates include the five events of the 2000 Saint-Ursanne sequence with additional events selected from the SED Bulletin that are less than 10 km in depth and that are found within a 5 km radius around Saint-Ursanne (Lat. 47.367°, Lon. 7.168°, Additional file 1: Table S2). To this subset of preselected templates, we then added, as template candidates, the 24 events from the combined Stuttgart—Seismic Solution catalogue (Additional file 1: Tables S3, S4). For these events, as their locations have higher uncertainties, we relaxed the template selection criteria and allowed as templates events located within a 10 km radius of Saint-Ursanne. Not all the microseismicity is visible on all 6 stations. Consequently, each station has a different number of initial templates.

The 20-year-long template matching scan at station BOURR identified 43 additional events that are well correlated with the 2000 sequence (Fig. 3). Of these, only one event with a CC of 0.83 was found post 2014 (i.e., after the installation of the dense local monitoring network). This event occurred on August 30th, 2017 at 05:56:31.8 (Fig. 3) and has an estimated magnitude of 0.7 M_{LX} (see Hermann et al., 2019 for details on the magnitude estimation). A small sequence in 2009 is linked to the M_L 2.9 event of May 20th, 2009. However, with calculated focal depths around 7 km, these events seem to be related to seismicity within the pre-mesozoic basement. Other events identified with the augmented array operative from 2014 onwards did not produce significant template matches and thus do not seem to be related to the 2000 Saint-Ursanne sequence; therefore, they are not considered further. Additional file 1: Fig. S1 shows the time history of earthquake detection for the MTI-Net stations. In both 2015 and 2017 we see few templates that show similarities with small cluster of events, but they are temporally confined and it is unsure if

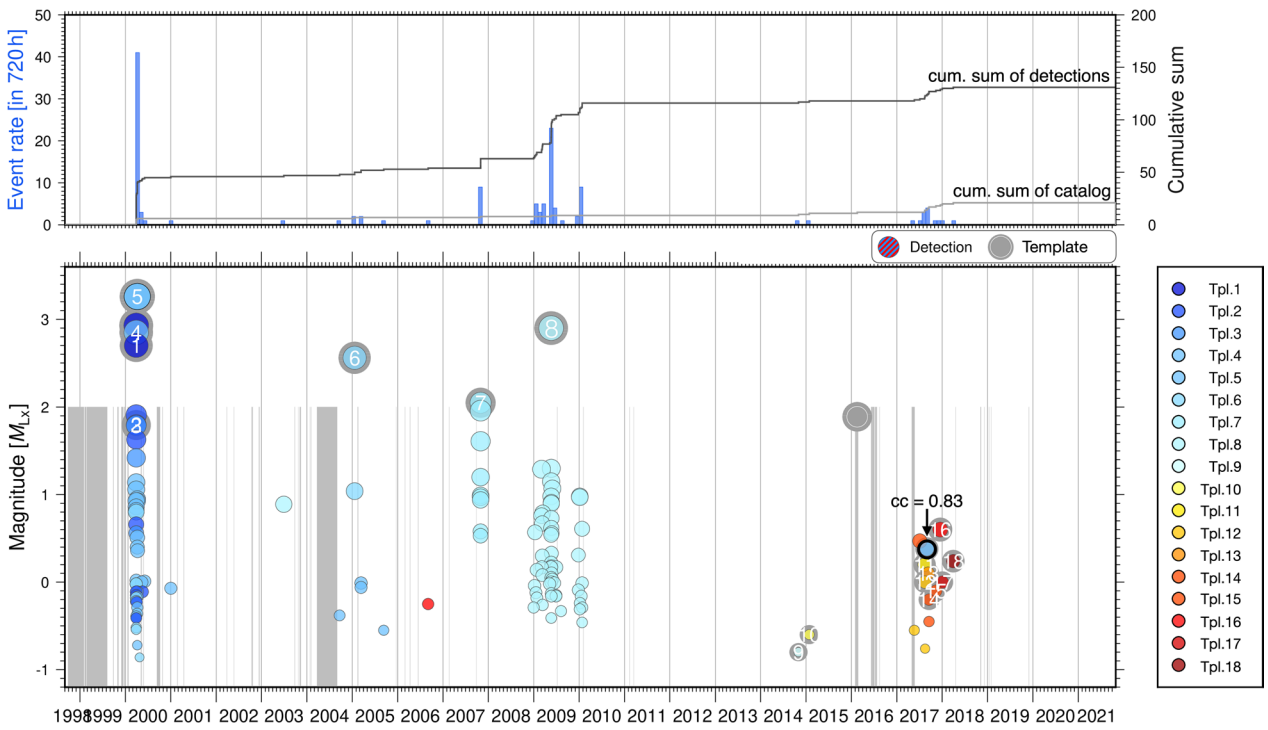

Fig. 3 Time line of template matching earthquake detections for station BOURR using using thresholds individually selected for each template family by visual inspection. Top panel: resolved event rate; the gray curves represent the cumulative number of events considering new detections (dark gray) and catalog events only (light gray). Coloring of events indicates to which template a detected event is most similar. Existing catalogue events are highlighted with a grey ring. A black ring indicates event 2017/08/30 05:56:32. Data gaps are indicated by vertical gray bars. Their height is a conservative estimate of the completeness magnitude of the SED catalog for the study area. Above this magnitude threshold earthquakes in the study area would have been detected without the template matching method

these burst of seismicity are linked to tunnel-related activities or natural diffuse seismicity. It is clear however, that the results from the template matching scans imply that the activity of the seismic sequence observed in 2000 remained very low since then. Consequently, because of the scarcity of detected events, it was not possible to obtain additional information about the orientation of the fault plane associated with the Saint-Ursanne sequence.

4.2 High-precision hypocenter relocations

All locations for events within a 10 km radius from Saint-Ursanne listed in the SED bulletin catalogue, including event 2017/08/30 which was found from our template matching analysis, are recalculated here using a newly developed Pg + Sg 3-D velocity model (Fig. 4; Diehl et al., 2021). This new model focuses on the velocity structure of the uppermost crust of the Central Alps and their foreland and allows for an increased accuracy of absolute earthquake locations. Relocations have been carried out using the NonLinLoc algorithm. The relocated events are listed in Additional file 1: Table S6. Figure 4 shows the derived absolute earthquake relocations. The horizontal and vertical uncertainties obtained from the probabilistic location procedure are displayed as error ellipses and bars, respectively and are on the order of 1–2 km (Fig. 4).

These locations were then used as initial input for hypoDD (v2.1b), which uses the double-difference algorithm of Waldhauser and Ellsworth (2000) with a regional 1-D velocity model (Diehl et al., 2021) and cross-correlation differential times to produce final high-precision relative hypocenter locations following the procedure described by Diehl et al. (2017). The events from the Saint-Ursanne sequence are relocated at very shallow depth, < 1 km Below Sea Level (BSL) (magenta circles, Fig. 5), although, because the boundary between the Paleozoic crystalline basement and sediments is very shallow in this region, some ambiguity remains. Moreover, because of the scarcity of events and relatively few differential times measured by cross-correlation, uncertainties in relative focal depths are too high to constrain the dip direction of the active fault in 2000 unambiguously: both a low-angle thrust fault dipping towards NNW and a steeply dipping reverse fault dipping towards SSE are consistent with the geometry highlighted by the relocations (Fig. 5).

4.3 Synthetic waveform modeling

In general, a precise and accurate focal depth can only be determined if an accurate velocity model is available and the distance between the epicenter and the closest station is not larger than about 1.5 times the focal depth (e.g., Diehl et al., 2021; Gomberg et al., 1990). In the case of the Saint-Ursanne sequence of the year 2000, the closest station at that time was BOURR, located ~ 5 km from the epicenter. For such a shallow sequence, this is unlikely sufficient to achieve a focal depth accuracy < 0.5 km, necessary to uniquely determine the lithology hosting this sequence. In an attempt to constrain the focal depth further and following the work by Kastrup et al. (2007) on the Fribourg sequences of 1987, 1995 and 1999, we searched the recorded seismograms for additional later-arriving seismic phases, which, when compared to synthetic seismograms, could help to discriminate between a source in the sedimentary layers and in the Paleozoic crystalline basement. Kim et al. (2006) and Ma and Atkinson (2006) demonstrated that so-called regional depth phases, such as the sPmP can be used to constrain focal depth. The sPmP is an S-wave radiated upwards to the Earth's surface where part of it is converted to a P-wave that is reflected downwards to the Moho where it is reflected as a PmP back to the Earth's surface (see the sketch in Fig. 6b). The travel-time difference between the sPmP and the direct PmP recorded at a given seismometer situated at the appropriate epicentral distance is very sensitive to the focal depth. For the calculation of synthetic seismograms, we used the program package REFMET by Ungerer (1990) and Forbriger (2003), which is based on the reflectivity method (Fuchs, 1968; Müller, 1985). REFMET requires a 1-D velocity model and different layering was tested to investigate the effects of a smooth, average regional versus a more detailed, local velocity model on the obtained synthetic seismograms. Results from these tests show that while the number of layers does not have a major influence on the seismograms, including a low-velocity zone is effective in better reproducing the S waves signal observed in the data. Therefore, we opted for a 1-D velocity model that is closest to the known crustal structure in the area of investigation. Figure 6a shows the 12-layer model obtained by integrating NAGRA borehole logs in NE Switzerland (Weber et al., 1986) and geological formations in the area, which was chosen for the final calculation. In the velocity profile, the depth of the top-basement of ~ 0.9 km BSL is consistent with the formation thicknesses in the region of Saint-Ursanne as shown in Nussbaum et al. (2017) where the top-basement is found to be at ~ 0.55 km BSL (see also Fig. 11), as well as with the model of Rime et al. (2019) further to the southwest of Saint-Ursanne, where the top-basement is located at ~ 1.3 km BSL. As a source for the synthetic seismograms, we used the moment tensor solution obtained for the mainshock of the sequence by J. Braunmiller (Fig. 9, see Sect. 4.5). Synthetics were calculated for an average 1-D crustal model along a profile with a forward azimuth of ~ 65° from Saint-Ursanne (Fig. 6c) and compared to the waveforms from

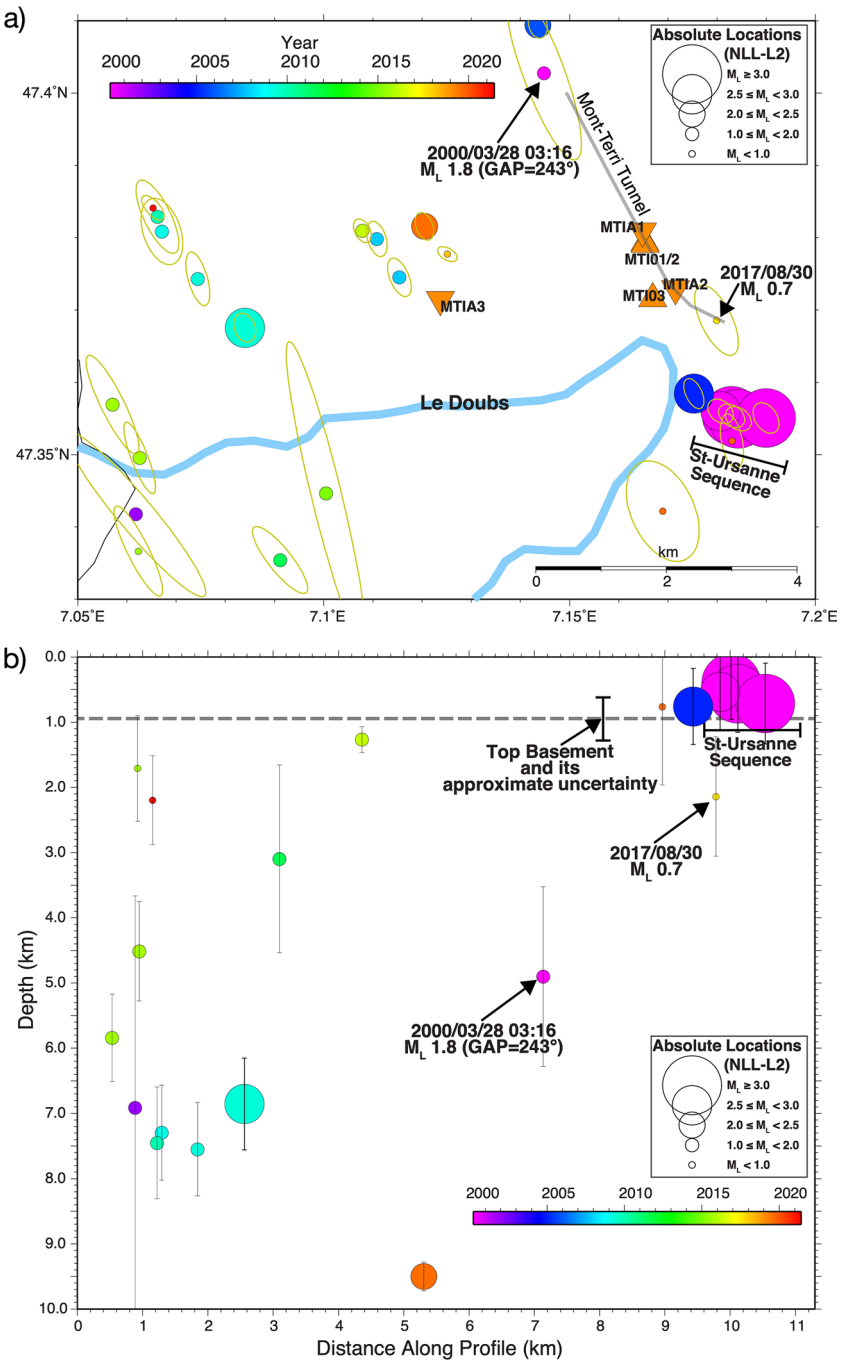

Fig. 4 Absolute relocations for shallow earthquakes listed in the SED catalogue from 2000 to 2021 (May 26th) in map view **a** and along an E-W profile **b** including only events of **a** with focal depths ≤ 10 km BSL. This includes also the event of August 2017, which was found through cross-correlation. In **a** we show NonLinLoc horizontal error ellipses. Vertical bars indicate the absolute uncertainty of focal depths. The gray, dashed line indicates the approximate top-basement at ~ 0.9 km depth BSL as inferred by integrating data from geological formations thickness of the area (Nussbaum et al., 2017) as well as the closest borehole logs in the NE (Weber et al., 1986) and in the SW of Saint-Ursanne (Rime et al., 2019)

the main shock of the Saint-Ursanne sequence (M_L 3.2 event of 2000/04/06 00:46:6.0) recorded at the equivalent distances along the same profile (Fig. 6d).

As expected, the travel-time difference in Fig. 7 between the sPmP and the PmP increases with focal depth, and the synthetic seismograms show that we

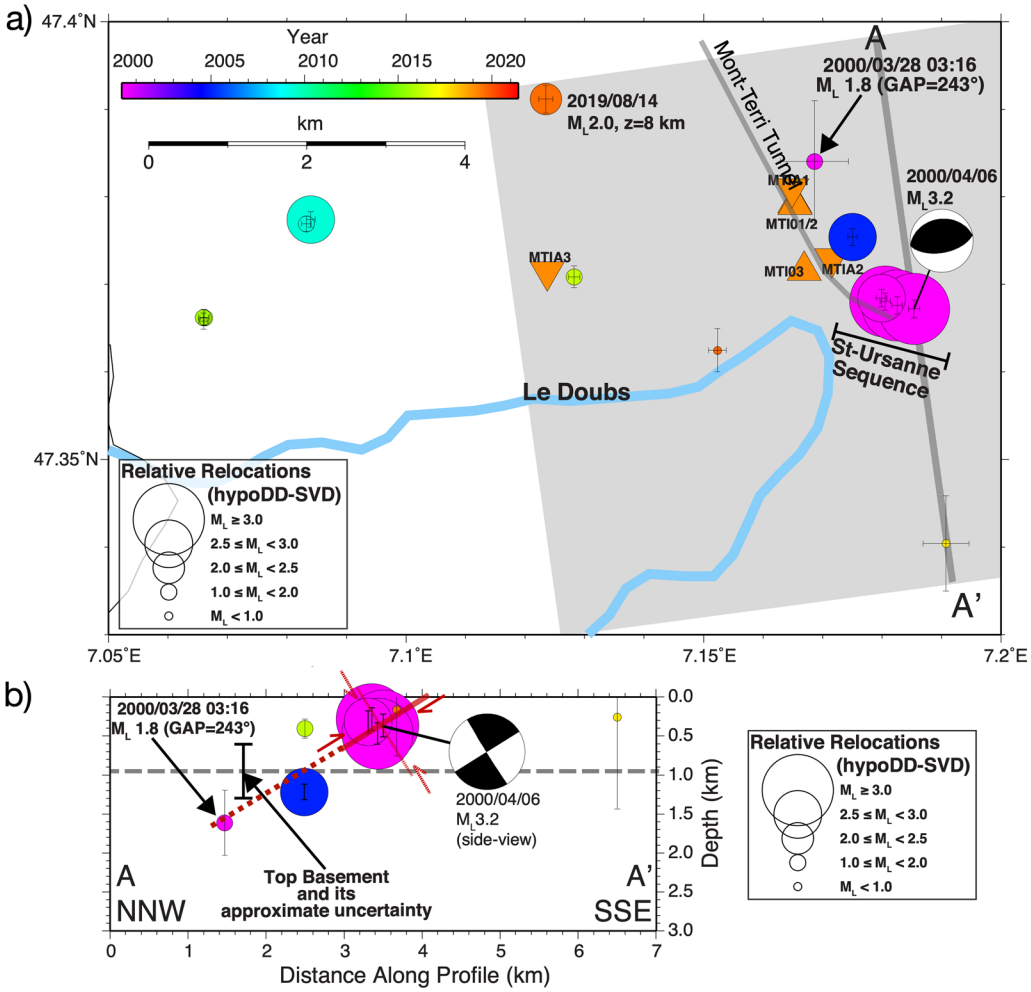

Fig. 5 Relative relocations for shallow earthquakes listed in the SED catalogue from 2000 to 2021 in map view **a** and along a depth-profile (**b**), oriented perpendicular to the strike of the focal planes. Note that the depth range focuses on the uppermost crust with only events with focal depths < 3 km BSL shown in the profile. No vertical exaggeration has been used for the cross section profile, thus the projection represents true dip angles. Relocations were obtained using the hypoDD algorithm of Waldhauser and Ellsworth (2000) using Singular-Value-Decomposition (SVD) inversion. Error bars indicate the horizontal and vertical relative location uncertainties derived by the SVD inversion. The gray, dashed line indicates the approximate top-basement at ~ 0.9 km depth BSL as inferred by integrating data from geological formations thickness of the area (Nussbaum et al., 2017) as well as the closest borehole logs in the NE (Weber et al., 1986) and in the SW of Saint-Ursanne (Rime et al., 2019)

should see two separate phases even for a focal depth as shallow as 1 km. However, a distinct second phase following the PmP cannot be identified either at station FELD or at station CHE (Fig. 7). The absence of the sPmP per se might not be considered a strong argument in favor of a very shallow focal depth, as the sPmP phase could be hiding in the signal-generated noise due to reverberations in the sedimentary layers below the stations. However, if we consider only stations that are located on outcropping crystalline basement and that have low background noise (i.e., FELD), we observe that also at these stations, the sPmP is not present. Moreover, in the context of a similar exercise, Kastrup et al. (2007) show an example of an earthquake at a depth of 2 km with an observed signal in which the sPmP is clearly visible. This argues in favor of our hypothesis that the M_L 3.2 event of 2000 was most likely not located in the Paleozoic crystalline basement, but rather in the overlying sediments. In a qualitative way, such a very shallow source is consistent also with the observation of a strong, long-lasting surface wave component typical of blasts located at the Earth's surface (e.g., Fig. 2). As shown in Fig. 8, the waveforms of deeper events (and thus in the Paleozoic crystalline basement) in 2009 and 2015 show very different waveform characteristics compared to the shallow events in 2000 and 2005, with less pronounced surface waves and higher

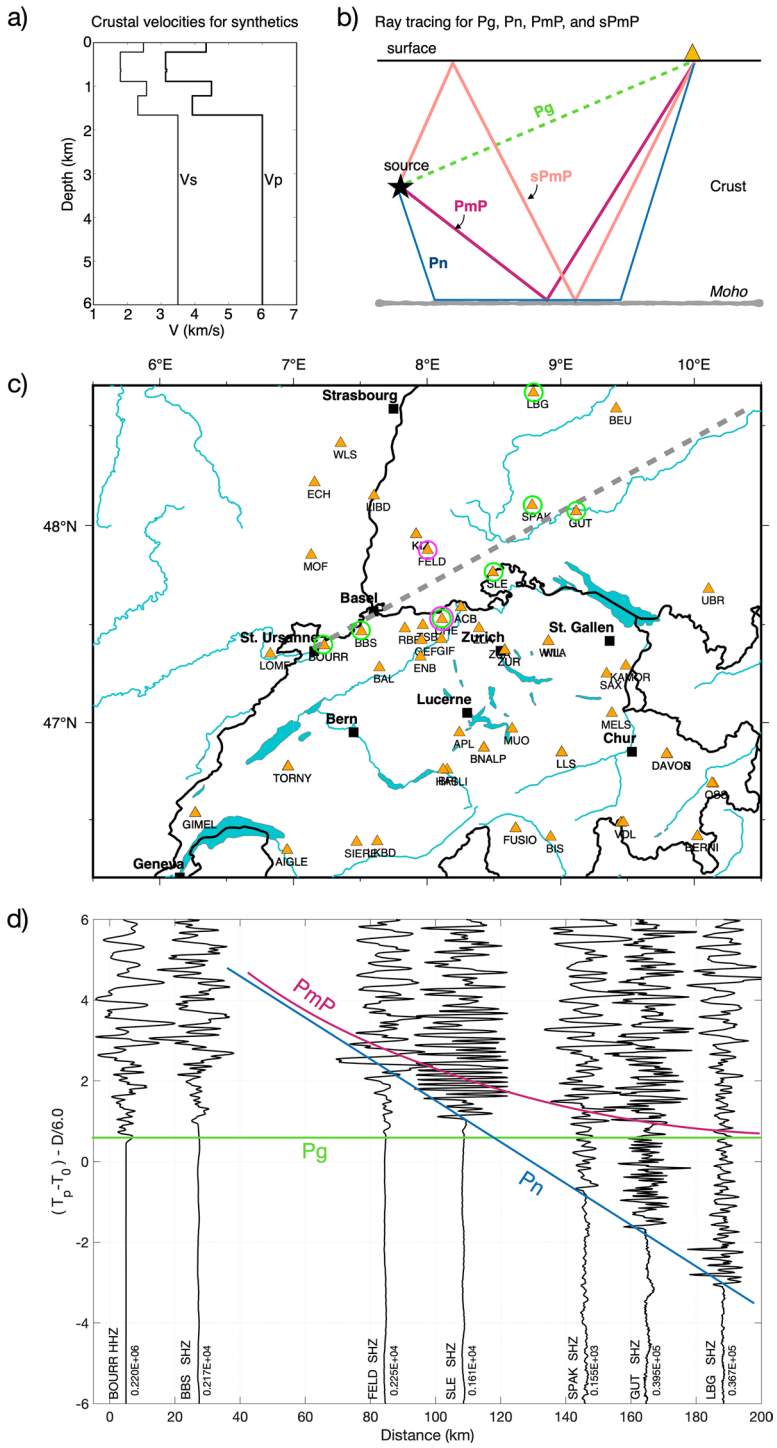

Fig. 6 **a** P-wave and S-wave velocities of the sedimentary cover around Saint-Ursanne estimated from NAGRA borehole logs in NE Switzerland. The average velocity is 4.2 km/s. **b** Diagram of Pg, Pn, PmP, and sPmP rays travelling through the crust from the hypocenter (star) to the station (triangle). **c** Recording stations during the 2000 sequence. Dashed line indicates the profile used in the calculation for the synthetic modelling. Stations shown in Fig. 7 are circled in magenta, whereas green circles indicate the stations shown in d). d) Reduced travel times (Vred = 6.0 km/s) as a function of epicentral distance (D) along the profile in the NE direction shown in (**c**) for real data from the main shock of the Saint-Ursanne sequence (M_L 3.2 event of 2000/04/06 00:46:6.0). Arrivals along the green horizontal line have an apparent velocity of 6.0 km/s and have travelled through the upper crust (Pg). The arrivals along oblique lines beyond about 120 km are Pn arrivals, indicating arrivals refracted at the Moho. Note the relatively emergent Pg-onsets at the first three stations compared to the relatively strong and impulsive Pn-onsets beyond 140 km

frequencies, as well as Sp precursor phases arriving prior to the direct Sg phase. Such Sp phases are generated by conversion at the basement-sediment interface and have been observed for instance for events in the Fribourg fault zone (e.g., Diehl et al., 2021).

On the other hand, our computations of synthetic seismograms with the REFMET algorithm failed to reproduce the pronounced surface waves seen in the recorded seismograms for stations close to the epicenter of the sequence (i.e., BOURR). Increasing the slowness range when calculating the synthetic seismograms does not provide a solution as it merely increases numerical artifacts. As previously mentioned, different velocity models (e.g., including/excluding the low-velocity zone) and layering were tested; however, we still weren't able to reproduce the surface waves components at closer stations. The failure in reproducing the surface wave component could be due to the simplifying assumptions of the

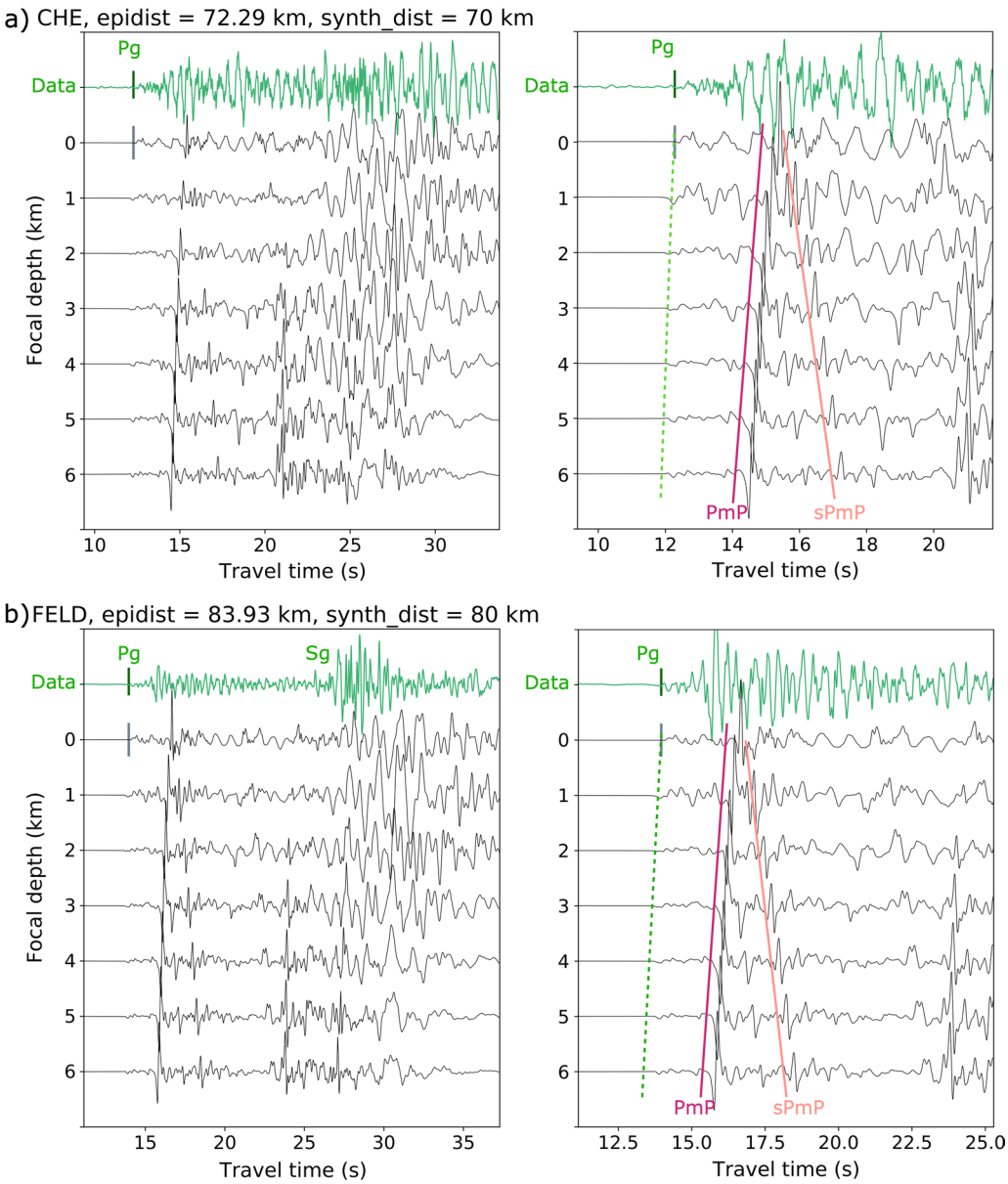

Fig. 7 Synthetic waveform modelling at stations CHE (distance ~ 70 km) and FELD (distance ~ 80 km). The right panel shows a zoom-in view around the P arrival time of the panel on the left. In each panel the top trace (green)represents the vertical component of the M_L 3.2 event of 2000 recorded at both CHE and FELD, respectively, whereas the bottom traces are synthetic seismograms for focal depths 0–6 km. Note how the sPmP is not visible in the data, matching the synthetic seismograms for depth shallower than 1 km

reflectivity method and/or the failure to reproduce 2-D or 3-D resonance effects. The latter could be ascribed to the presence of Permo-Carboniferous troughs that have been inferred to characterize this portion of the Jura FTB under the Saint-Ursanne region (e.g., Leu, 2008). Future testing could involve numerical simulations of seismic-wave propagation that supports a fully 3-D heterogeneous material model such as the software SW4 (Petersson & Sjögreen, 2017).

4.4 Focal mechanism

A first focal mechanism for the strongest event of the sequence (M_L 3.2) was obtained from a full-waveform moment tensor (MT) inversion (J. Braunmiller, pers. Comm.). The resulting focal mechanism corresponds to a reverse fault with one fault plane dipping steeply to the south and the other dipping gently to the north (Fig. 9). The best fit between the observed signals and the synthetics is obtained for a moment magnitude, M_w, of 3.3 and for a focal depth of 2 km. Although the depth resolution of the moment tensor inversion is not sufficient to discriminate between a source within the sedimentary cover and a source in the underlying Paleozoic crystalline basement, the resulting focal depth agrees to first order with the hypothesis of a shallow source. The MT solution, however, is constrained by only few stations and the signal-to-noise ratios in the frequency range used for the MT inversion are rather low due to the relatively small magnitude of the event (Fig. 9). We therefore consider the MT solution to be of low quality.

Since first-motion fault-plane solutions of dip-slip reverse- or normal-faulting mechanisms are very sensitive to the vertical take-off angles and since these take-off angles will result in significantly different solutions for a source in the Paleozoic crystalline basement compared to a source in the lower-velocity sedimentary cover, the focal mechanism depends strongly on the focal depth and the velocity model. However, as shown by the examples in Fig. 10a–c, previous attempts to better constrain the focal depth by comparing the fit of fault-plane solutions for different focal depths and different velocity models were not conclusive.

In this study, we reconstructed the focal mechanism for the largest (M_L 3.2) event of April 6th, 2000 of the sequence. In our case, the take-off angles were computed with the NonLinLoc software, using the Pg + Sg 3-D velocity model of Diehl et al. (2021) with the hypocenter in the sedimentary cover (0.7 km BSL). Depth is obtained from the derived absolute earthquake relocation and it is consistent with the synthetic waveform modeling that also argue for a source in the sediments. For our calculation, we used the HASH algorithm (Hardebeck & Shearer, 2002), which provides uncertainties shown by a set of acceptable solutions (gray lines in Fig. 10d). Following the definition of Aki and Richards (2002), the parameters strike, dip and rake are used here to define fault-orientations.

The strike, dip and rake of the nodal planes of the preferred focal mechanism averaged over all accepted solutions are 080/58/098 and 262/32/092 (Fig. 10d). Thus, the solution represents either an SSE-dipping steep reverse fault or an NNW-dipping low-angle thrust fault. This is in agreement with the solution from the moment tensor inversion (Fig. 9), with both solutions derived from full-moment tensor inversion and first-motion polarities, showing a dominant thrust component.

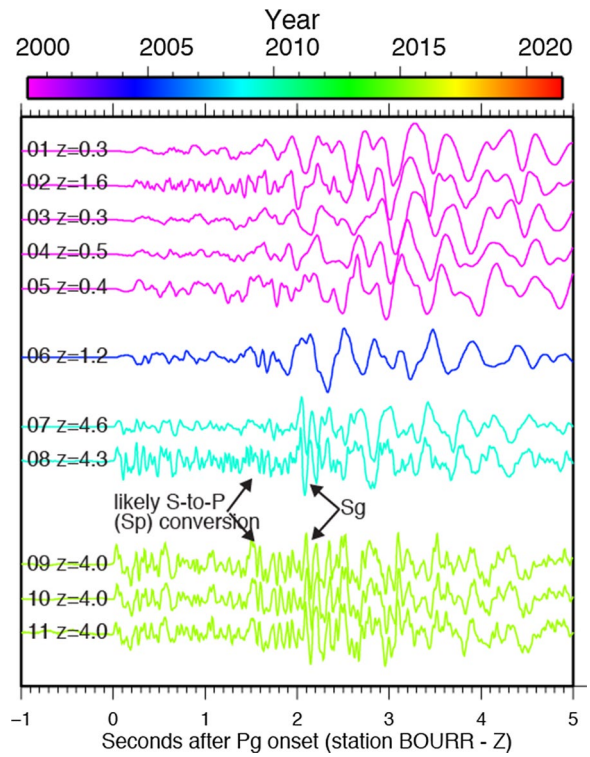

Fig. 8 Vertical-component waveforms of selected earthquakes in the the Saint-Ursanne region recorded at station BOURR. Z is the focal depth in kilometers resulting from the relative relocations shown in Fig. 5. Colors denote origin time. Note the differences in waveform characteristics between near-surface sources (event 1–6, including the sequence of 2000) and sources likely located in the Paleozoic crystalline basement (event 7–11). See text for details

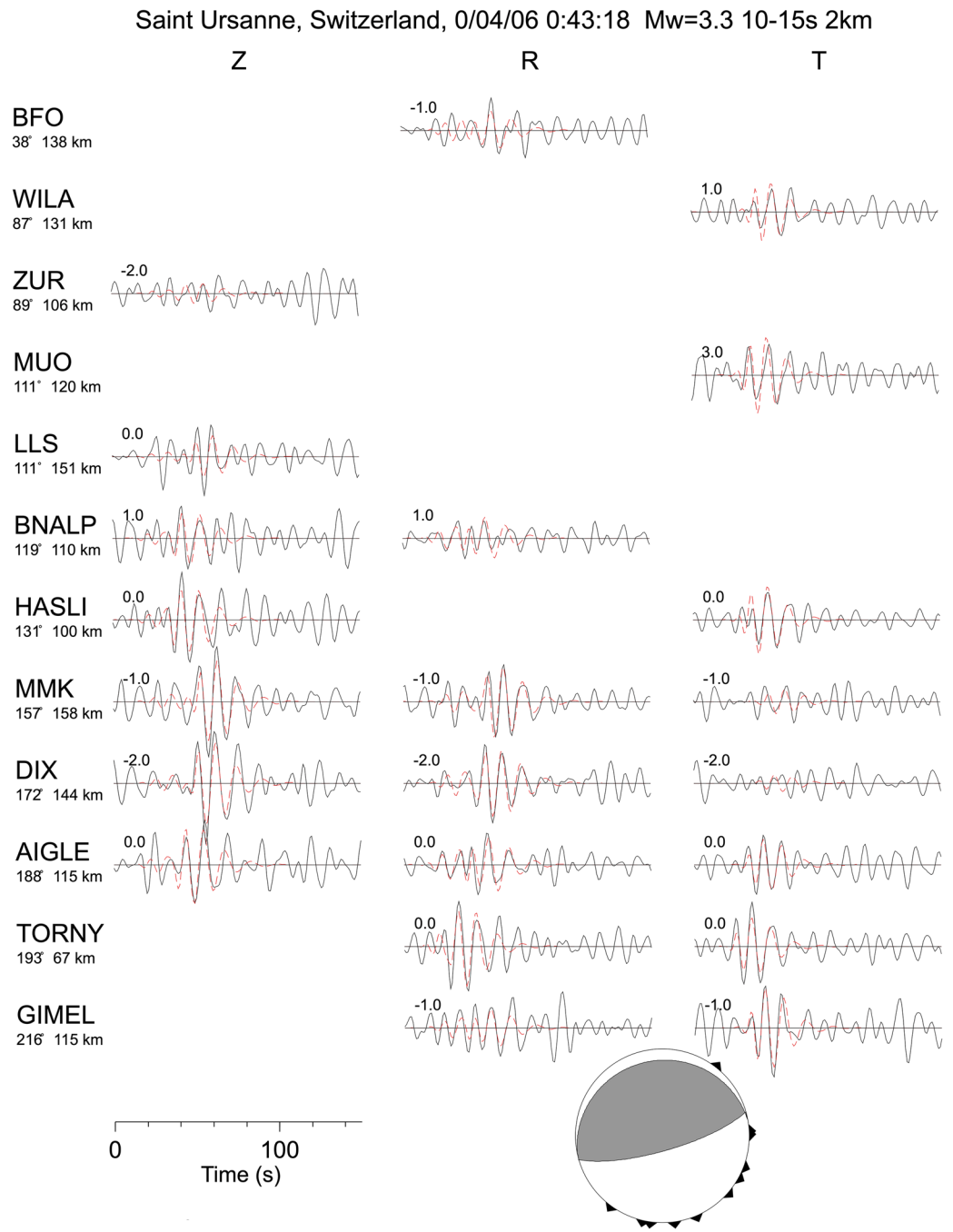

Fig. 9 Full-waveform moment-tensor solution for the mainshock of the Saint-Ursanne seismic sequence (April 6th, 2000). The strike, dip and rake of the two nodal planes are 074/076/89 and 259/014/95. From J. Braunmiller (pers. Comm.)

5 Results

5.1 Summary of the evidence for a source in the sedimentary cover

The reanalysis of the earthquake sequence of the year 2000 near Saint-Ursanne has yielded three lines of argument to constrain the focal depth:

1. The strong surface waves observed at small epicentral distances that are usually associated with quarry blasts (Figs. 2 and 8);
2. The high-precision relocations with an improved 3-D P- and S-velocity model that result in a focal depth of less than 1 km BSL (Figs. 4 and 5);

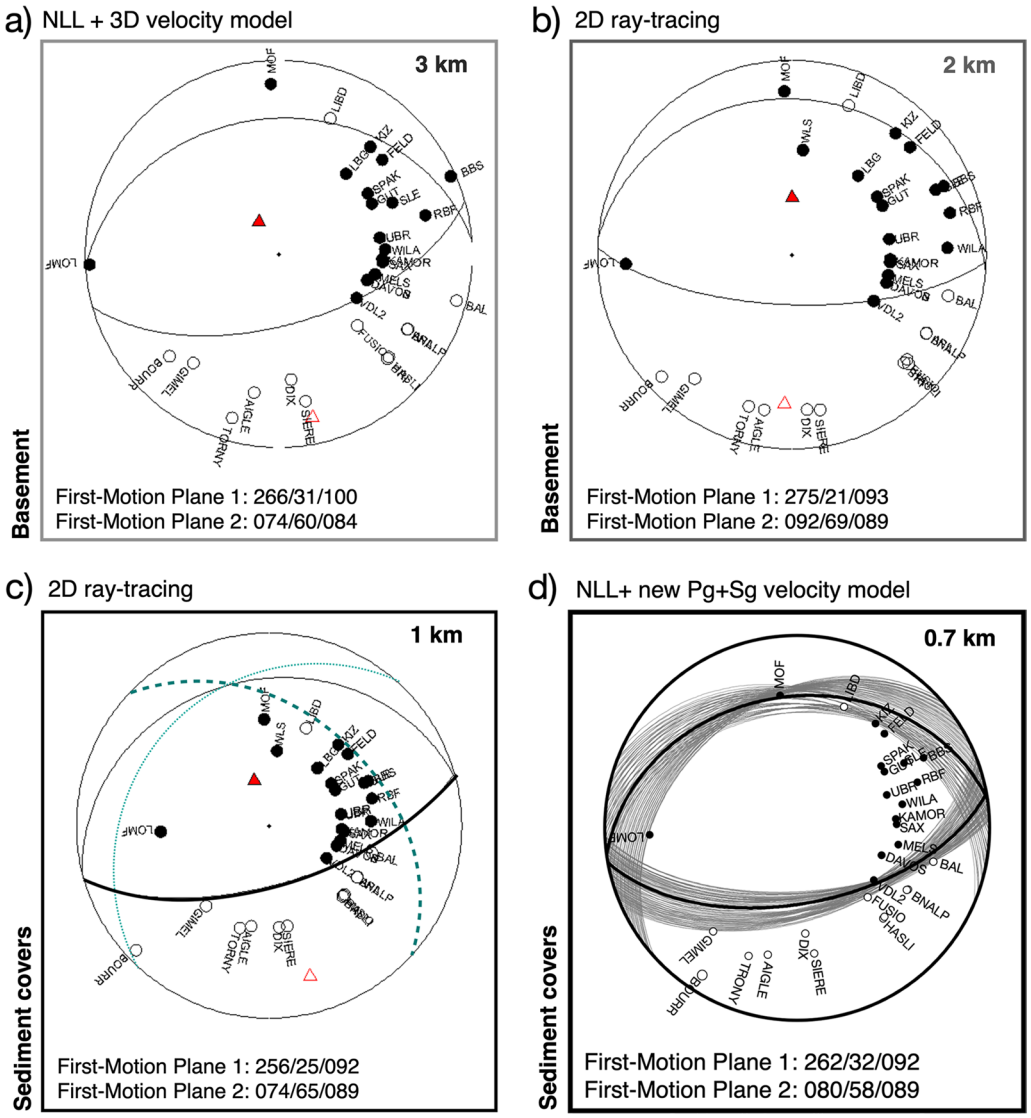

Fig. 10 First-motion focal mechanisms solutions for the M_L 3.2 event of April 6th, 2000 based on **a** take-off angles calculated routinely with NonLinLoc (NLL) and the 3-D model of Husen et al. (2003); **b** take-off angles based on 2-D ray-trace models for focal depths in the basement (2 km); **c** and in the sediments (1 km); here with different lines styles and colors are indicated those nodal plane solutions for which an equally good fit is obtained. **d** take-off angles calculated with NonLinLoc, the new 3-D Pg + Sg model (Diehl et al., 2021) and a focal depth of 0.7 km BSL. Stereogram is lower hemisphere, equal-area projection. Solid circles correspond to compressive first motion (up); empty circles correspond to dilatational first motion (down). Grey lines in d) show sets of acceptable solutions derived by the HASH algorithm (Hardebeck & Shearer, 2002); black bold lines indicate the (preferred) average focal mechanism of all accepted solutions. For all cases, strike, dip, and rake of the two focal planes are provided below each mechanism

3. The synthetic seismogram modelling, which indicates that the absence of the sPmP in the observed seismograms requires a source at or very close to the Earth's surface (Fig. 7).

Although it can be objected that each one of these three lines of argument alone is not sufficiently convincing, together they constitute three independent and consistent pieces of evidence for an exceptionally shallow source. Thus, the Saint-Ursanne sequence of the year 2000 represents a relatively rare case of ongoing seismicity in the sedimentary cover of the northern Jura FTB.

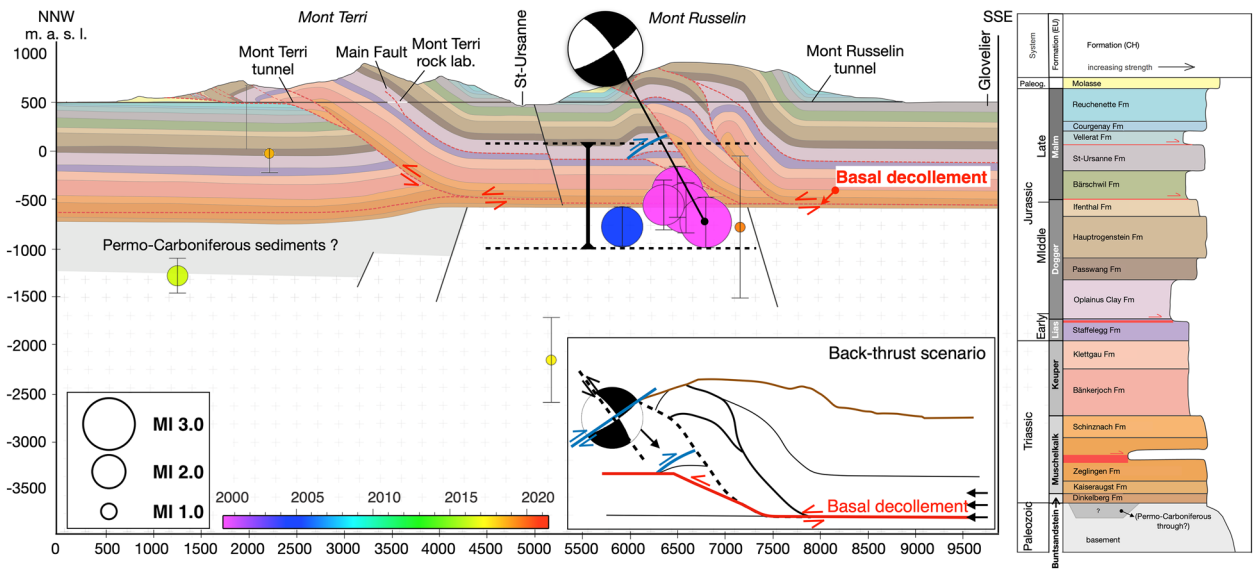

Fig. 11 Forward modelled NNW-SSE cross section along the Mont Terri tunnel from Nussbaum et al. (2017). Absolute locations obtained in this study (see Fig. 4 for details) for shallow earthquakes are overlaid. Vertical bars indicate absolute errors of focal depths. The thick error bar indicates the combined depth uncertainties obtained from both absolute and relative relocations. Colors indicate origin time. Size of symbols is proportional to magnitude. The focal mechanism of the strongest event based on first-motion polarities suggests a north-dipping low-angle thrust mechanism. As the sense of motion disagrees with the basal decollement, a backthrust rooting in the top of the Lias Group (Staffelegg Formation in the Lithostratigraphic Lexicon of Switzerland) in the footwall of the Mont Russelin ramps is more likely to be the active plane of the 2000 seismic sequence. Note that the lexicon of the lithostratigraphic column follows the lexicon of Switzerland. The corresponding European lexicon of the lithostratigraphic groups for the Triassic and Jurassic epochs is also indicated. For more information about the definition of the units in the Lithostratigraphic Lexicon of Switzerland, as well as further cross-links to other units, please visit www.strati.ch. Figure modified from Nussbaum et al. (2017)

5.2 The active fault plane for the Saint-Ursanne sequence of 2000

Based on the best-fitting focal mechanism, we can choose between an active fault plane dipping with 58° towards the SSE and a fault plane dipping with 32° towards the NNW. If one projects this mechanism on the geological cross-section shown in Fig. 11, one is tempted to associate the steeper SSE dipping plane with the prominent fault at the northern foot of Mont Russelin. However, based on mechanical considerations, it is very unlikely that this fault could have been activated by the Saint-Ursanne earthquake sequence. In fact, Sibson (1990) provides a simple two-dimensional analysis of the stress ratio required for the reactivation of faults of different orientations. Given the shallow focal depth of the Saint-Ursanne events and the nearly pure thrust-fault focal mechanism, the least compressive stress must be vertical, and fluid pressures are at most hydrostatic. Assuming furthermore that the coefficient of friction on the fault is about 0.75, Fig. 2 of Sibson (1990) shows that faults with a dip greater than about 53° are so unfavorably oriented that they are essentially locked. Such faults can only become active under conditions of lithostatic or supra-lithostatic fluid pressures. The same applies to the corresponding fault plane of the moment tensor with an even steeper dip (Fig. 9). On the other hand, the same argument shows that both the 32° dip of the other fault plane of the first-motion solution and the 14° dip of the corresponding moment-tensor fault plane are well within the range of faults optimally oriented for reactivation under the given stress regime. Therefore, we conclude that the earthquake sequence of Saint-Ursanne occurred as SSE directed slip of the hanging wall on a fault that dips gently to the NNW. In addition, if one would assume that the 2005 event (blue circle in Fig. 5) occurred on the same fault as the events of the year 2000—as the continuation of the NNW plane seem to suggest (red dashed line in Fig. 5b)—then the NNW low-angle fault would again provide a better match than the steep SSE dipping plane. If slip occurred on an NNW low-angle fault, because the detachment between the Mesozoic sediments and the underlying pre-mesozoic basement gently dips SSE, it implies that the Saint-Ursanne sequence cannot be associated with slip along the décollement, but rather that it corresponds to a form of back-thrusting within the sedimentary cover. This scenario is in agreement with the kinematic forward modelling from Nussbaum et al. (2017) where the final model shows a backthrust

is initiated at the top of the Lias Group (Staffelegg Formation, Fig. 11). Another possible alternative is that the Saint-Ursanne sequence is linked to a duplex ramp geometry. Indeed, although the development of internal duplexes in the Upper Triassic units was not integrated in the forward modelling, it could also fit our observations as duplex ramps would lead to a similar geometry with back-thrusting in the Jurassic units of the Lias Group (Staffelegg Formation). Nussbaum et al. (2017) noted, however, that there is no field evidence to date of such duplex ramps or inherited basement faults that could have triggered the duplexes.

6 Discussion

6.1 Evidence for active thrust-faulting in the sediment cover of the northern segment of the Jura fold-and-thrust belt

We have shown that the deformation associated with the Saint-Ursanne sequence represents a rare example of active compression; is there any additional evidence for depth-dependent variations in the stress field of the northern Jura FTB? We have compiled all the available focal mechanism solutions associated with the seismicity in our study area from 1984 to date (Fig. 12) based on the compilation by Kastrup et al. (2004) and the annual earthquake reports of the SED, complemented with recent (unpublished) solutions. At the south-eastern edge of the Rhine Graben, in the Basel region, we observe a NW–SE striking cluster composed of earthquakes whose focal depths range from 5 to 20 km. This seismicity is partly associated with the northern tip of the Basel-Läufelfingen Lineament described in Diehl et al. (2021). At these depths, the predominant style of deformation indicated by these earthquakes is a strike-slip to transtensive regime (Fig. 12). For earthquakes distributed in the pre-mesozoic basement in the north-eastern part of the Jura FTB, the center part of our study region, we observe a similar pattern of predominantly transtensive mechanisms (Fig. 12). As for the sedimentary cover, the scarcity of seismic data and the ambiguity due to hypocenter uncertainties have so far impeded the discrimination between earthquakes within cover sequences and upper crustal events, and thus to differentiate between the corresponding style of deformation (Rabin et al., 2018). Our analysis positions the Saint-Ursanne sequence (URS in Fig. 12), at depths shallower than 1 km and assigns it a thrust mechanism. Similarly, a possible source in the Mesozoic sediments has been proposed for the recent M_L 2.8 Grenchen event of 2017 (GRE in Fig. 12) by Diehl et al. (2021). A near-surface source is indicated by strong surface waves similar to quarry-blast signals as well as by focal depths derived with the Pg + Sg relocation procedure of Diehl et al. (2021). The Grenchen event locates SE from Saint-Ursanne (Fig. 12), in the transition between the Jura-FTB and the Molasse Basin, in-between the Weissenstein- and Arch-Anticline (e.g., Meier 2010). Similar to the Saint-Ursanne sequence, the first motion focal mechanism derived for the Grenchen event of 2017, indicates reverse faulting. The shallower plane dipping about 25° towards SE was preferred as the active fault plane with respect to the mechanically unlikely steep (65°), NW dipping plane. In this case, however, the SE-dipping, low-angle thrust fault might very well be associated with the main basal Jura FTB décollement or a secondary thrust, located above the main décollement level. Another recent example of a possible shallow transpressive event occurred in February 2021 near Neuchâtel (NEC in Fig. 12). The focal depth derived with the relocation procedure of Diehl et al. (2021) indicates a near-surface location as well, with the shallower plane dipping about 40° towards NNW. Therefore, the Saint-Ursanne, the Grenchen and the Neuchâtel earthquakes bear witness of active thrust faulting within the Jura FTB and support the notion of a seismically active contraction in the northwestern Alpine foreland of Switzerland.

6.2 Stress field rotation between the basement and the sediments of the northern segment of the Jura fold-and-thrust belt

Considering these recent signs of active thrust faulting in the sediment cover of the northern tip of the Jura FTB, we now explore what are the implications for the style of deformation, stress field and coupling/decoupling between sediments and basement in the corresponding region.

We observe how stress inversion of focal mechanism data (Rabin et al., 2018; cyan lines in Fig. 13) show a σ_1 orientation which differs from the near-surface interpolated maximum horizontal stress (σ_{Hmax}) orientation by about 30°: the σ_1 from the stress inversion has a NW–SE orientation, whereas the near-surface stress averages out to a N-S direction (Becker, 2000; Reinecker et al., 2003, red butterflies and arrows in Fig. 13). In the stress inversion of Rabin et al. (2018), the σ_1 directions for earthquakes both in the cover and in the basement share a fairly similar orientation, although the authors admit that, due to hypocenter uncertainties, they cannot unambiguously separate earthquakes within cover sequences from upper crustal events. For the Saint-Ursanne event (URS), the P-axis derived from our analysis shows a slight rotation in the N-S direction (Fig. 13) in agreement with the average of the near-surface in-situ measurements (Becker, 2000), as well as with the shortening directions obtained from paleostress (post 2.9 Ma) fault-slip data

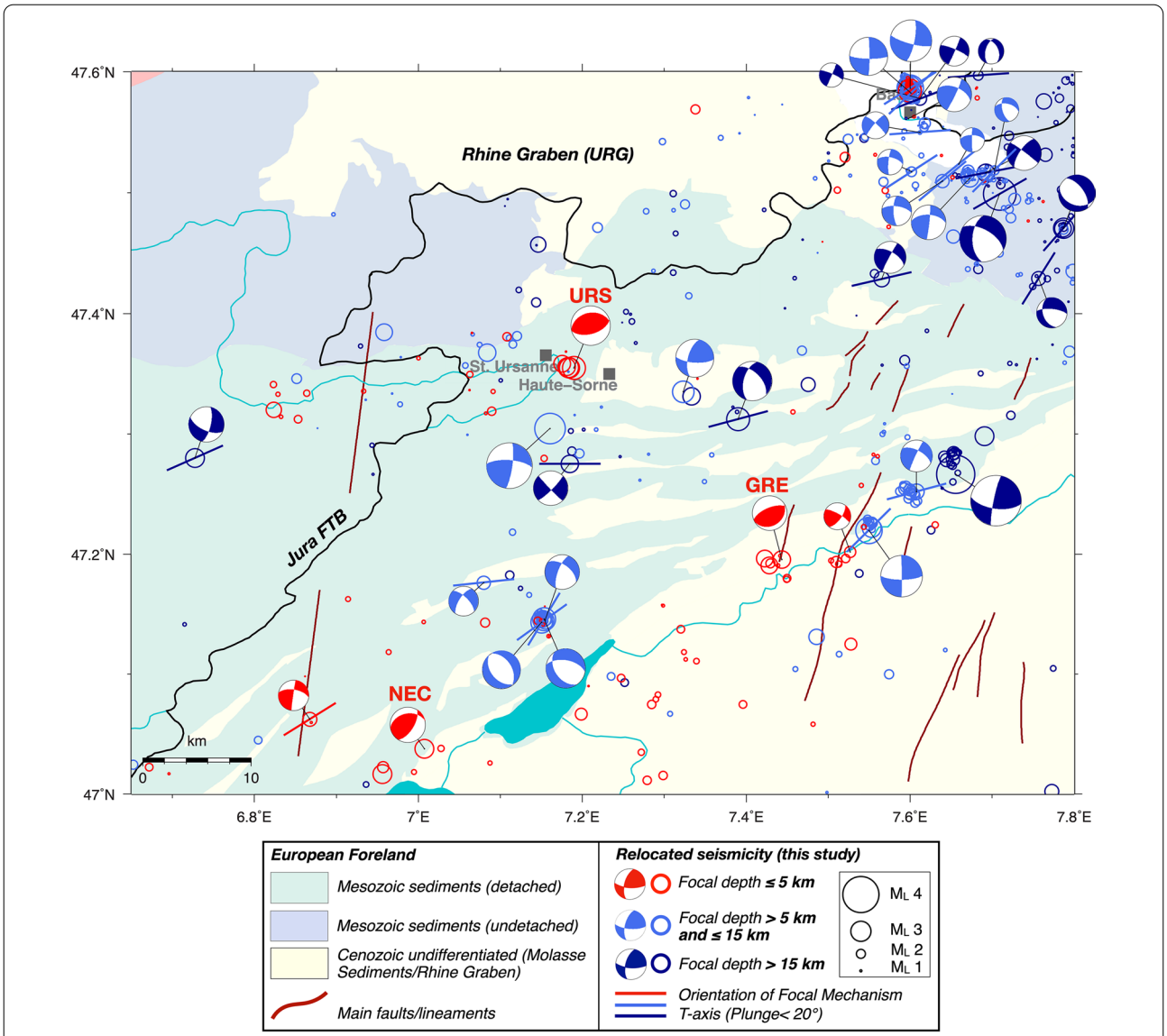

Fig. 12 Epicenters and focal mechanisms of earthquakes recorded by the Swiss Seismological Service in the northern tip of the Jura FTB between 1984 and 2021 (May 26th). Locations are absolute relocations obtained using the new 3D Pg + Sg velocity model of Diehl et al. (2021). Events and focal mechanisms discussed in the text (bold labels) are Saint-Ursanne (URS), Grenchen (GRE), Neuchâtel (NEC). T axes with plunge ≤ 20° are also plotted color-coded by the depths of the associated earthquakes. Background colors outline major tectonic units. Red lines indicate faults adopted from Heuberger et al. (2016), Mock and Herwegh (2017), Vouillamoz et al. (2017) and Swisstopo (2005)

(Ustaszewski & Schmid, 2006, 2007; white small arrows in Fig. 13). This is also consistent with the stress measurements carried out in borehole BDS-5 at Derrière Mont Terri by the method of hydraulic fracturing (Jaeggi & Bossart, 2016). From their analysis, the stress tensor derived in the Upper Jurassic limestones indicate a nearly N-S thrusting, with an σ_H orientation of N14° ± 19°, in line with the Saint-Ursanne sequence. This rotation however is less evident for the other two shallow events analyzed in this study (GRE and NEC) whose P-axes have a rather NW–SE orientation, in agreement with the σ_1 direction from the stress inversion of Rabin et al. (2018). Thus, in the northern Jura FTB, the Saint-Ursanne event seems to indicate that within the cover rocks no detectable reorientation of the maximum horizontal compression (σ_{Hmax}) has occurred since the onset of thin-skinned Jura FTB folding, and that the anticlockwise rotation of present-day σ_{Hmax} rotation from cover to basement indicates ongoing mechanical decoupling of the sedimentary cover from its basement along Mid- to Late Triassic

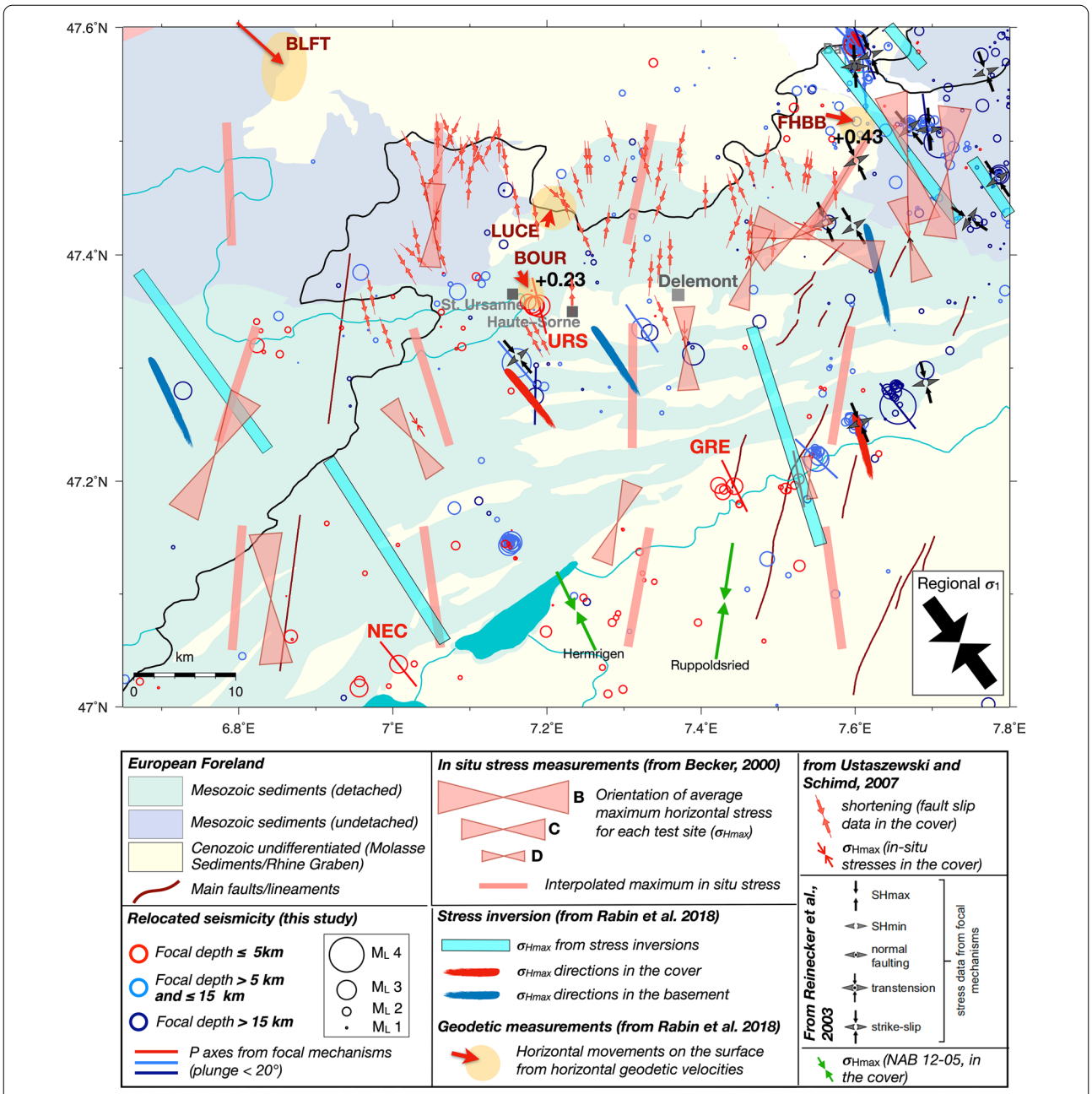

Fig. 13 Summary of in-situ stress measurements from Becker (2000), stress inversion from Rabin et al. (2018), paleostress fault-slip data (post 2.9 Ma) from Ustaszewski and Schmid (2006), stress data from the 2003 release of the World Stress Map project (Reinecker et al., 2003), data from Nagra drill sites Hermrigen and Ruppoldsried (Heidbach & Reinecker, 2013), and P-axes derived in this study. Please refer to the legend for symbols explanations. Note that σ_{Hmax}-orientations regarding recent near-surface deformation (in situ measurements, red butterfly symbols) tend to scatter between NNW and NNE, paralleling the shortening directions determined from the fault-slip data (white arrows). σ_{Hmax}-orientations obtained from seismic activity within the Paleozoic crystalline basement (black arrows), however, are predominantly and more systematically NW–SE-oriented

weak layers, in agreement with Ustaszewski and Schmid (2007). On the other hand, the Neuchâtel and Grenchen events, which are located at the transition between Jura FTB and the Molasse Basin show little evidence for the present-day rotation seen in the northern Jura FTB (Saint-Ursanne), while their style of deformation differs from that of the basement. A report on the analysis of the stress field conducted in Northern Switzerland by Nagra in 2013 (Arbeitsbericht NAB 12–05, Heidbach & Reinecker, 2013) also shows that at the southern boundary

of our area of investigation (drilling sites Hermrigen and Ruppoldsried, Fig. 13) there is no statistically significant σ_{Hmax} rotation with depth, thus indicating that contemporary mechanical decoupling is not very efficient in this region.

To better investigate the potential difference between the deformation in the shallow crust and in the deeper part of the basement, we show the deformation style in terms of the rake angles, following the representation adopted in Delacou et al. (2004) in Fig. 14. We converted the rake angle for each known focal mechanism into a scalar rake value S ranging between -1 (pure normal) to +1 (pure reverse), with $S=0$ corresponding to pure strike-slip following the definition of Mazzotti et al. (2021). If the active plane is known from relative relocations, we use the corresponding S value, otherwise we use the mean S of both planes. The obtained S values are assigned a magnitude weighting (e.g., $M_L \geq 3.5$ are weighted 3 times more than events smaller than M_L 2.5), and they are spatially interpolated for two different depth intervals (Fig. 14a, b). We first consider events with focal depths between 0 and 5 km, in order to represent the uppermost crust (Fig. 14a), and then compare the results with those obtained only from events whose locations are between 5 and 15 km (the upper crust, Fig. 14b). While we observe that compression is the dominant style of deformation for the shallow crust (0 to 5 km), areas with extensional regime (e.g., the region of Biel in Fig. 14b) are related to sequences located at > 10 km depth, in the Paleozoic crystalline basement (e.g., Diehl et al., 2015). Whether such decoupling is indicative of ongoing thin-skinned tectonics is a different matter: some authors (Becker, 2000; Ustaszewski & Schmid, 2007) reject the thin-skinned hypothesis as characteristic of the neotectonic style of deformation in the Jura FTB, as decoupling can be also expected in a thick-skinned scenario according to analog modeling (Mosar, 1999; Ustaszewski et al., 2005a).

Without entering in the debate thin-skinned versus thick-skinned, our work provides new reliable evidence that the present-day stress field in our study area is inhomogeneous, with σ_{Hmax} being NW–SE-oriented in the basement, but N-S in the covers at least in the northern Jura FTB. Although only few focal mechanisms are presently available in the shallowest part of the crust (close to the Jura FTB-decollement and even shallower), they indicate a tendency for ongoing reverse-thrusting. This is observed both in the northern Jura FTB (URS in Fig. 12) and close to the transition to the Molasse Basin (GRE and NEC in Fig. 12). Due to the rather small number of reliable focal mechanisms in the region, it remains however unclear how present-day shortening of Jura FTB is accommodated and partitioned between strike-slip fault systems mapped by structural data and thrust faulting

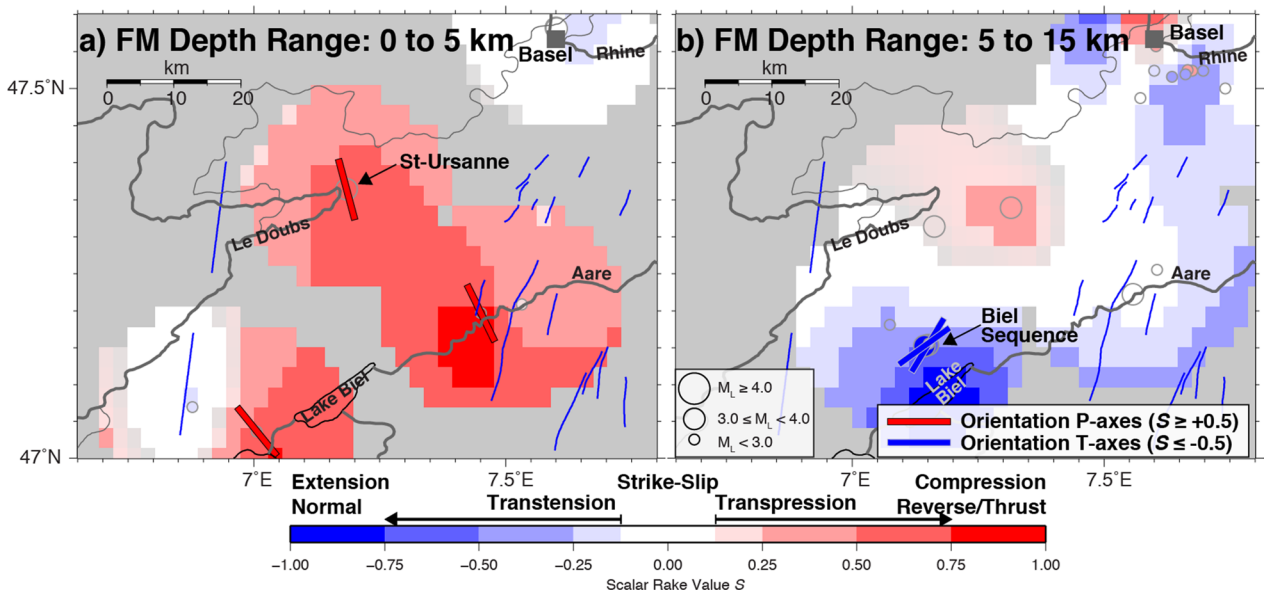

Fig. 14 Regionalization of the deformation in the northern Jura FTB (*S* parameter, based on the rake angle, see text) for two different depth intervals within the upper crust. **a** Uppermost crust (0–5 km). **b** Upper to mid-crustal depths (5–15 km). The colour code corresponds to the type of deformation (compression in red, extension in blue, strike-slip in white). Circles are observed focal mechanism (FM) color-coded according to the *S* values, same as the interpolated grid in the background. The orientation of T-axes for extensional and the orientation of the P-axes for compressional focal mechanisms are also shown with blue and red lines, respectively

observed from seismicity. It is thus possible that thrust events accommodate only a small portion of the present-day deformation within the cover. Major strike-slip faults, such as the Pontarlier fault (e.g., Radaideh & Mosar, 2021), however, also exhibit a rather low level of seismic activity over the past thirty-five years (e.g., Diehl et al., 2021) and similarly few strike-slip focal mechanisms are associated with sources in the sedimentary cover of the Jura FTB. On the other hand, a transtensional regime clearly prevails in deeper parts of the Paleozoic crystalline basement below the Jura FTB, including normal-fault and strike-slip mechanisms (Fig. 12).

Thus, our conclusion differs from the study of Rabin et al. (2018), who argue for a rather homogeneous stress tensor with depth and a general NW–SE compressional orientation in the northern part of the Jura FTB, affecting the cover and the basement under a general strike-slip regime. However, the three shallow thrust events (URS, GRE, NEC) presented here were not available at the time of their study, so that they were not able to carry out a separate stress analysis for the sedimentary cover. We also note here that the number of these shallow events is currently rather small as well as their event magnitudes. Therefore, the uncertainty of the derived P-axis is not well-constrained, and more focal mechanisms will be needed to provide more robust estimates. However, the fact that we have found only three such shallow thrust events over the past 20 years is consistent with the very low deformation rates, likely below 0.5 mm/yr as suggested by the horizontal geodetic velocities (Fig. 13; Brockmann et al., 2012; Houlié et al., 2018; Rabin et al., 2018; Villiger, 2014).

7 Conclusions

Our re-analysis of the Saint-Ursanne sequence provides new evidence for present-day active thrust faulting in the Jurassic fold and thrust belt and its vicinity. This seismically active contraction in the northeastern segment of the Jura FTB finds confirmation also in the recent 2017 Grenchen and 2021 Neuchâtel earthquakes, both likely associated with low-angle thrusts as well. This constitutes a rare piece of evidence that the shallow portion of the Jura FTB is still in a compressional (thrust faulting) regime. With few exceptions in the eastern part of the Alpine front, there are almost no other purely compressional regions in Switzerland where thrust/reverse mechanisms are prevalent (Delacou et al., 2004; Kastrup et al., 2004; Rabin et al., 2018). On the other hand, our conclusions do not imply that the basement below the Jura FTB is aseismic. We find clear evidence in Saint-Ursanne and surrounding areas (e.g., Biel sequence, Läufelfingen sequence, Fig. 14) for seismicity within the Paleozoic crystalline basement, indicating presence of active faults. However, the stress field orientation differs. In the northernmost segment of the Jura FTB, from a comparison between our findings, published in-situ stress measurements (Becker, 2000), recent stress inversion, and geodetic measurements (Rabin et al., 2018), we observe a stress field rotation between the basement and the sedimentary cover. There, shallow near-surface thrusts show a slight rotation of P-axes in a N-S orientation rather than the typical NW–SE orientation at the Jura FTB transition to the Molasse Basin, and of the strike-slip and transtensive deformation that predominates the Paleozoic crystalline basement. As proposed also by Rabin et al. (2018) on the basis of their geodetic measurements, this argues for a mechanical decoupling of the cover from its basement for the northernmost portion of the Jura FTB.

In conclusion, our analysis highlights a superposition of various mechanisms in the Jura FTB, with a remaining reverse-thrust regime partly accommodating ongoing shortening of the Jura FTB in the shallow part likely imposed by classic thin-skinned mechanisms, and a transtensive regime in the deeper parts of the basement. As proposed by Singer et al., (2014) and Kissling and Schlunegger (2018), a possible model explaining the observed transtensional regime in the basement could be related to large-scale geodynamic processes such as roll-back dynamics of the European slab. We show that tectonic deformation in both the sedimentary cover and the basement is present and ongoing. Even though the deformation rate is rather low, as attested by the few small to moderate earthquakes recorded in the last decades, these aspects must be considered in the hazard and risk assessment of potential geotechnical projects targeting the uppermost crust in the northeastern part of the Jura FTB.

Supplementary Information

The online version contains supplementary material available at https://doi.org/10.1186/s00015-021-00400-x.

Additional file 1. Additional tables and figures.

Acknowledgements

Comments by two anonymous reviewers and Naomi Vouillamoz helped to improve the manuscript and are thankfully acknowledged. We thank Jochen Braunmiller for providing the moment tensor solution used in this study. We acknowledge the collaboration with permanent seismic networks used in this study: CH (Swiss Seismological Service & ETH Zurich, 1983), FR (Reseau sismologique et géodésique français (RESIF), 1995), LE (Landesamt für Geologie & Rohstoffe Und Bergbau, 2009), RA (Reseau sismologique et géodésique français (RESIF), 1995).

Authors' contributions

FL: Conceptualization, Data curation, Formal analysis, Visualization, Writing-original draft, Writing-review and editing. TD: Funding acquisition, Conceptualization, Visualization, Supervision, Writing—review and editing. ND: Code resources, Writing—review and editing. TK: Code resources, Writing—review and editing. CN: Writing—review and editing. SS: Writing—review and editing.

SW: Funding acquisition, Writing—review and editing. All authors read and approved the final manuscript.

Funding
Open access funding provided by Swiss Federal Institute of Technology Zurich. Financial support for the research presented in this study and the operation of seismic stations in the study region was provided by the Federal Office of Topography (swisstopo). This work was also supported by the Swiss Geophysical Commission in the framework of the SeismoTeCH project and the Nationale Genossenschaft für die Lagerung radioaktiver Abfälle (Nagra).

Availability of data and materials
Waveform data from the SED permanent seismic network (network codes CH) as well as the majority of waveform data collected by collaborating networks (network codes FR, RA, LE, GR) in the greater Alpine region are openly available through the European Integrated Data Archive (EIDA): http://www.orfeus-eu.org/data/eida/. The SED now provides open access to station inventory and earthquakes catalogues via the International Federation of Digital Seismograph Networks (FDSN) webservices (http://www.seismo.ethz.ch/en/research-andteaching/products-software/fdsn-web-services/ for details).

Declarations

Competing interests
The authors declare that they have no known competing financial interests or personal relationships that could have appeared to influence the work reported in this paper.

Author details
[1]Swiss Seismological Service, Swiss Federal Institute of Technology, ETH Zürich, Sonneggstrasse 5, 8092 Zürich, Switzerland. [2]Swiss Geological Survey, Federal Office of Topography, Swisstopo, Seftigenstrasse 264, 3084 Wabern, Switzerland.

Received: 15 August 2021 Accepted: 10 December 2021
Published online: 06 January 2022

References

Abednego, M., Blascheck, P., Schefer, S., Nussbaum, C., Joswig, M., Bossart, P., & Mosar, J. (2017). Seismotectonic analysis around the Mont Terri rock laboratory (Switzerland): A pilot study. *Swiss Journal of Geosciences, 110*, 233–251. https://doi.org/10.1007/s00015-017-0263-6

Affolter, T., & Gratier, J. P. (2004). Map view retrodeformation of an arcuate fold-and-thrust belt: The Jura case. *Journal of Geophysical Research, 109*, B03404. https://doi.org/10.1029/2002JB002270

Aki, K., & Richards, P. G. (2002). *Quantitative seismology* (2nd ed., p. 704). University Science Books.

Aubert, D. (1949). Le Jura. *Geologische Rundschau, 37*, 2–17. https://doi.org/10.1007/BF01792491

Baer, M., Deichmann, N., Braunmiller, J., Ballarin Dolfin, D., Bay, F., Bernardi, F., Delouis, B., Fäh, D., Gerstenberger, M., Giardini, D., et al. (2001). Earthquakes in Switzerland and surrounding regions during 2000. *Eclogae Geologicae Helvetiae, 94*, 253–264.

Becker, A. (2000). The Jura Mountains: An active foreland fold-and-thrust belt? *Tectonophysics, 321*, 381–406. https://doi.org/10.1016/S0040-1951(00)00089-5

Blascheck, P. (2018). Gefährdung von Endlagern für radioaktive Abfallstoffe durch Kleinstbeben und deren Überwachung mittels Nanoseismic Monitoring. PhD Thesis, Institute for Geophysics, University of Stuttgart.

Bläsi, H. R., Peters, T. J., & Mazurek, M. (1991). Der Opalinus Clay des Mont Terri (Kanton Jura): Lithologie, Mineralogie und physiko-chemische Gesteinsparameter. Nagra Interner Bericht, 90–60, 44 pp. Nagra, Wettingen, Switzerland.

Bossart, P., & Thury, M. (2008). Mont Terri rock laboratory. Project, programme 1996–2007 and results. Reports of the Swiss Geological Survey, No. 3, 445 pp. Federal Office of Topography (swisstopo), Wabern, Switzerland.

Bossart, P., Bernier, F., Birkholzer, J., Bruggeman, C., Connolly, P., Dewonck, S., Fukaya, M., Herfort, M., Jensen, M., Matray, J.-M., et al. (2017). Mont Terri rock laboratory, 20 years of research: Introduction, site characteristics and overview of experiments. *Swiss Journal of Geosciences, 110*, 3–22. https://doi.org/10.1007/s00015-016-0236-1

Brockmann, E., Ineichen, D., Marti, U., Schaer, S., Schlatter, A., & Villiger, A. (2012). Determination of Tectonic Movements in the Swiss Alps Using GNSS and Levelling. *Geodesy for Planet Earth* (pp. 689–695). Springer. 10.1007/978-3-642-20338-1_85.

Burkhard, M. (1990). Aspects of the large-scale Miocene deformation in the most external part of the Swiss Alps (Subalpine Molasse to Jura fold belt). *Eclogae Geologicae Helvetiae, 83*, 559–583.

Buxtorf, A. (1907). *Geologische Beschreibung des Weissenstein-Tunnels und seiner Umgebung. Beiträge zur Geologischen* (p. 147). Karte der Schweiz, NF 21.

CH—Swiss Seismological Service (SED) at ETH Zurich. (1983). National seismic networks of Switzerland. *ETH Zürich*. https://doi.org/10.12686/sed/networks/ch

Deichmann, N. (1990). *Seismizität der Nordschweiz, 1980–1988, und Auswertung der Erdbebenserien von Günsberg* (p. 90). Nagra Technischer Bericht, Wettingen: Läufelfingen und Zeglingen, 90-46.

Deichmann, N., Diehl, T., & Braunmiller, J. (2012). The earthquake sequences of Saint Ursanne. *SED-ETHZ, Zürich, 21*(04), 2012.

Delacou, B., Sue, C., Champagnac, J.-D., & Burkhard, M. (2004). Present-day geodynamics in the bend of the western and central Alps as constrained by earthquake analysis. *Geophysical Journal International, 158*(2), 753–774. https://doi.org/10.1111/j.1365-246X.2004.02320.x

Dèzes, P., Schmid, S. M., & Ziegler, P. A. (2004). Evolution of the European Cenozoic Rift System: Interaction of the Alpine and Pyrenean orogens with their foreland lithosphere. *Tectonophysics, 389*, 1–33. https://doi.org/10.1016/j.tecto.2004.06.011

Diehl, T., Clinton, J., Cauzzi, C., Kraft, T., Kästli, P., Deichmann, N., Massin, F., Grigoli, F., Molinari, I., Böse, M., Hobiger, M., Haslinger, F., Fäh, D., & Wiemer, S. (2021). Earthquakes in Switzerland and surrounding regions during 2017 and 2018. *Swiss Journal of Geosciences, 114*, 4. https://doi.org/10.1186/s00015-020-00382-2

Diehl, T., Clinton, J., Deichmann, N., Cauzzi, C., Kastli, P., Kraft, T., Molinari, I., Bose, M., Michel, C., Hobiger, M., et al. (2018). Earthquakes in Switzerland and surrounding regions during 2015 and 2016. *Swiss Journal of Geosciences, 111*, 221–244. https://doi.org/10.1007/s00015-017-0295-y

Diehl, T., Clinton, J., Kraft, T., Husen, S., Plenkers, K., Guilhelm, A., Behr, Y., Cauzzi, C., Kaestli, P., Haslinger, F., Faeh, D., Michel, C., & Wiemer, S. (2014). Earthquakes in Switzerland and surrounding regions during 2013. *Swiss Journal of Geosciences, 107*(359–375), 1091. https://doi.org/10.1007/s00015-014-0171-y

Diehl, T., Deichmann, N., Clinton, J., Kaestli, P., Cauzzi, C., Kraft, T., Behr, Y., Edwards, B., Guilhem, A., Korger, E., Hobiger, M., Haslinger, F., Faeh, D., & Wiemer, S. (2015). Earthquakes in Switzerland and surrounding regions during 2014. *Swiss Journal of Geosciences, 108*, 425–443. https://doi.org/10.1007/s00015-015-0204-1

Diehl, T., Kissling, E., Herwegh, M., & Schmid, S. (2021). Improving absolute hypocenter accuracy with 3-D Pg and Sg body-wave inversion procedures and application to earthquakes in the central alps region. *Journal of Geophysical Research: Solid Earth*. https://doi.org/10.1029/2021JB022155

Diehl, T., Kraft, T., Kissling, E., & Wiemer, S. (2017). The induced earthquake sequence related to the St. Gallen deep geothermal project (Switzerland): Fault reactivation and fluid interactions imaged by microseismicity. *Journal of Geophysical Research: Solid Earth, 122*, 7272–7290. https://doi.org/10.1002/2017JB014473

Forbriger, T. (2003). Notizen zur Berechnung synthetischer Seismogramme mit der Reflektivitatsmethode. Report, BFO Schiltach, Germany.

Freivogel, M., & Huggenberger, P. (2003). Modellierung bilanzierter Profile im Gebiet Mont Terri-La Croix (Kanton Jura). In: P. Heitzmann & J.-P. Tripet (Eds.), Mont Terri Project-geology, paleohydrology and stress field of the Mont Terri region, Geology Series, (pp.7–44). Federal Office for Water and Geology (FOWG), Vol. 5, 319 pp.

FR—RESIF. (1995), RESIF-RLBP French broad-band network, RESIF-RAP strong motion network and other seismic stations in metropolitan France. RESIF—Réseau Sismologique et géodésique Français. https://doi.org/10.15778/resif.fr

Fuchs, K. (1968). The reflection of spherical waves from transition zones with arbitrary depth-dependent elastic moduli and density. Special issue.

Journal of Physics of the Earth, 16, 27–41. https://doi.org/10.4294/jpe1952.16.Special_27
Giamboni, M., Ustaszewski, K., Schmid, S. M., Schumacher, M. E., & Wetzel, A. (2004). Plio-Pleistocene Transpressional Reactivation of Paleozoic and Paleogene Structures in the Rhine-Bresse transform Zone (northern Switzerland and eastern France). *International Journal of Earth Sciences, 93*, 207–223. https://doi.org/10.1007/s00531-003-0375-2
Giamboni, M., Wetzel, A., Nivière, B., & Schumacher, M. E. (2004). Plio-Pleistocene folding in the southern Rhinegraben recorded by the evolution of the drainage network (Sundgau area; Northwestern Switzerland and France). *Eclogae Geologicae Helvetiae, 97*, 17–31. https://doi.org/10.1007/s00015-004-1112-4
Gomberg, J. S., Shedlock, K. M., & Roecker, S. W. (1990). The effect of S-wave arrival times on the accuracy of the hypocenter estimation. *Bulletin of the Seismological Society of America, 80*, 1605–1628.
Hardebeck, J. L., & Shearer, P. M. (2002). A new method for determining first-motion focal mechanisms. *Bulletin of the Seismological Society of America, 92*, 2264–2276.
Heidbach, O., and Reinecker, J. (2013). Analyse des rezenten Spannungsfelds der Nordschweiz, (Nagra Arbeit Ber. NAB 12-05). Wettingen: Nagra.
Heim, A. (1919). Geologie der Schweiz. *Tauchnitz*. https://doi.org/10.3929/ethz-a-005780481
Henry, P., Deloule, E., & Michard, A. (1997). The erosion of the Alps: Nd isotopic and geochemical constraints on the sources of the peri-alpine molasse sediments. *Earth and Planetary Science Letters, 146*(3–4), 627–644. https://doi.org/10.1016/S0012-821X(96)00252-X
Herrmann, M., Kraft, T., Tormann, T., Scarabello, L., & Wiemer, S. (2019). A consistent high-resolution catalog of induced seismicity in Basel based on matched filter detection and tailored post-processing. *Journal of Geophysical Research: Solid Earth, 124*, 8449–8477. https://doi.org/10.1029/2019JB017468
Heuberger, S., Roth, P., Zingg, O., Naef, N., & Meier, B. P. (2016). The St Gallen Fault Zone: a long-lived, multiphase structure in the North Alpine Foreland Basin revealed by 3D seismic data. *Swiss Journal of Geosciences, 109*(1), 83–102. https://doi.org/10.1007/s00015-016-0208-5
Houlie, N., Woessner, J., Giardini, D., & Rothacher, M. (2018). Lithosphere strain rate and stress field orientations near the Alpine arc in Switzerland. *Sci Reports, 8*, 1–14. https://doi.org/10.1038/s41598-018-20253-z
Husen, S., Kissling, E., Deichmann, N., Wiemer, S., Giardini, D., & Baer, M. (2003). Probabilistic earthquake location in complex three-dimensional velocity models: Application to Switzerland. *Journal of Geophysical Research, 108*(B2), 2077–2096. https://doi.org/10.1029/2002JB001778
Jaeggi, D., & Bossart, P. (2016). Borehole BDS-5 near Derrière-Monterri, Courgenay, Switzerland. Synthesis report—Ber. Landesgeol. 6.
Jordan, P. (1992). Evidence for large-scale decoupling in the Triassic evaporites of Northern Switzerland: An overview. *Eclogae Geologicae Helvetiae, 85*, 677–693.
Joswig, M. (2008). Nanoseismic monitoring fills the gap between microseismic networks and passive seismic. *First Break, 26*, 121–128.
Kastrup, U., Deichmann, N., & Fröhlich, A. (2007). Evidence for an active fault below the northwestern Alpine foreland of Switzerland. *Geophysical Journal International, 169*(3), 1273–1288. https://doi.org/10.1111/j.1365-246X.2007.03413.x
Kastrup, U., Zoback, M. L., Deichmann, N., Evans, K. F., Giardini, D., & Michael, A. J. (2004). Stress field variations in the Swiss Alps and the northern Alpine foreland derived from inversion of fault plane solutions. *Journal of Geophysical Research, 109*, B01402. https://doi.org/10.1029/2003JB002550
Kim, W.-Y., Dineva, S., Ma, S., & Eaton, D. (2006). The 4 August 2004, Lake Ontario Earthquake. *Seismological Research Letters, 77*(1), 65–73. https://doi.org/10.1785/gssrl.77.1.65
Kissling, E., & Schlunegger, F. (2018). Rollback orogeny model for the evolution of the Swiss Alps. *Tectonics, 37*, 1097–1115. https://doi.org/10.1002/2017TC004762
Lacombe, O., Angelier, J., Byrne, D., & Dupin, J. (1993). Eocene-Oligocene tectonics and kinematics of the Rhine-Saône continental transform zone (Eastern France). *Tectonics, 12*, 874–888. https://doi.org/10.1029/93TC00233
Laubscher, H. P. (1961). Die Fernschubhypothese der Jurafaltung. *Eclogae Geologicae Helvetiae, 54*, 222–282.
Laubscher, H. P. (1963a). *Erläuterungen zum Geologischen Atlasblatt «1085 St-Ursanne, 1:25'000». Basel: Schweizerische Geologische Kommission*. Waber: Federal Office of Topography (swisstopo).
Laubscher, H. P. (1963b). *Geologischer Atlas der Schweiz, Atlasblatt 40, 1085 St. Ursanne-Erläuterungen Basel: Schweizerische Geotechnische Kommission*. Federal Office of Topography (swisstopo).
Laubscher, H. P. (1986). The eastern Jura: Relations between thin-skinned and basement tectonics, local and regional. *Geologische Rundschau, 75*, 535–553. https://doi.org/10.1007/BF01820630
Laubscher, H. P. (1997). The décollement hypothesis of the Jura folding after 90 years. *Bulletin of Applied Geology, 2*(2), 167–182.
Laubscher, H. P. (2010). Jura, Alps and the boundary of the Adria subplate. *Tectonophysics, 483*(3–4), 223–239. https://doi.org/10.1016/j.tecto.2009.10.011
Lebeau, R. (1951). Sur la structure du Jura: Les enseignements de l'excursion géologique interuniversitaire en Franche-Comté (31 août—6 septembre 1949). *Revue De Géographie De Lyon, 26*(1), 71–75. https://doi.org/10.3406/geoca.1951.6039
LE—Landesamt Fuer Geologie, Rohstoffe Und Bergbau. (2009). Landeserdbebendienst Baden-Wuerttemberg. *International Federation of Digital Seismograph Networks*. https://doi.org/10.7914/SN/LE
Leu, W. (2008). Permokarbon-Kartenskizze (Rohstoffe) Kompilation eines GIS-Datensatzes auf der Basis von bestehenden Unterlagen (Bereich Schweizer Mittelland). *Nagra Arbeitsbericht* (NAB 08–49). Wettingen: Nagra.
Lomax, A., Virieux, J., Volant, P., & Thierry-Berge, C. (2000). Probabilistic earthquake location in 3D and layered models. In C. H. Thurber & N. Rabinowitz (Eds.), *Advances in Seismic Event Location* (pp. 101–134). Kluwer Academic Publishers.
Lyon-Caen, H., & Molnar, P. (1989). Constraints on the deep structure and dynamic processes beneath the Alps and adjacent regions from an analysis of gravity anomalies. *Geophysical Journal International, 99*(1), 19–32. https://doi.org/10.1111/j.1365-246X.1989.tb02013.x
Ma, S., & Atkinson, G. M. (2006). Focal depths for small to moderate earthquakes ($mN \leq 2.8$) in western Quebec, southern Ontario, and northern New York. *Bulletin of the Seismological Society of America, 96*(2), 609–623. https://doi.org/10.1785/0120040192
Madritsch, H., Kounov, A., Schmid, S. M., & Fabbri, O. (2009). Multiple fault reactivations within the intra-continental Rhine-Bresse Transfer Zone (La Serre Horst, eastern France). *Tectonophysics, 471*(3–4), 297–318. https://doi.org/10.1016/j.tecto.2009.02.044
Madritsch, H., Schmid, S. M., & Fabbri, O. (2008). Interactions between thin- and thick-skinned tectonics at the northwestern front of the Jura fold-and-thrust belt (eastern France). *Tectonics, 27*(5), 1–31. https://doi.org/10.1029/2008TC002282
Mazzotti, S., Aubagnac, C., Bollinger, L., Oscanoa, K. C., Delouis, B., Paco, D. D., Doubre, C., Godano, M., Jomard, H., Larroque, C., Laurendeau, A., Masson, F., Sylvander, M., & Trilla, A. (2021). FMHex20: An earthquake focal mechanism database for seismotectonic analyses in metropolitan France and bordering regions. *Bulletin De La Société Géologique De France, 192*(1), 10. https://doi.org/10.1051/bsgf/2020049
Meier, B. P. (2010). Ergänzende interpretation reflexionsseismischer Linien zwischen dem östlichen und westlichen Molassebecken, Nagra Arbeitsbericht (vol. NAB 10–40, pp. 48). Nagra, Wettingen, Switzerland.
Mock, S., & Herwegh, M. (2017). Tectonics of the central Swiss Molasse Basin: Post-Miocene transition to incipient thick-skinned tectonics? *Tectonics, 36*(9), 1699–1723. https://doi.org/10.1002/2017TC004584
Mosar, J. (1999). Present-day and future tectonic underplating in the western Swiss Alps: Reconciliation of basement/wrench-faulting and decollement folding of the Jura and Molasse basin in the Alpine foreland. *Earth and Planetary Science Letters, 173*, 143–155.
Müller, G. (1985). The reflectivity method: A tutorial. *Journal of Geophysics., 58*, 153–174.
Müller, W. H., & Briegel, U. (1980). Mechanical aspects of the Jura overthrust. *Eclogae Geologicae Helvetiae, 73*, 239–250.
Nussbaum, C., Kloppenburg, A., Caër, T., & Bossart, P. (2017). Tectonic evolution around the Mont Terri rock laboratory, northwestern Swiss Jura: Constraints from kinematic forward modelling. *Swiss Journal of Geosciences, 110*, 39–66. https://doi.org/10.1007/s00015-016-0248-x
Pavoni, N. (1961). Faltung durch Horizontalverschiebung. *Eclogae Geologicae Helvetiae, 54*, 515–534.

Petersson, N. A., & Sjogreen, B. (2017). SW4, version 2.01 [software]. Computational Infrastructure of Geodynamics. https://doi.org/10.5281/zenodo.1063644
Pfiffner, O. A. (2017). Thick-skinned and thin-skinned tectonics: A Global perspective. *Geosciences, 7*(3), 71. https://doi.org/10.3390/geosciences7030071
Pfiffner, O. A., Erard, P., & Stäuble, M. (1997). Two cross sections through the Swiss Molasse Basin (lines E4–E6, W1, W7–W10). In O. A. Pfiffner, P. Lehner, P. Heitzmann, S. Mueller, & A. Steck (Eds.), *Deep structure of the Swiss Alps. Results of NRP 20* (pp. 64–72). Birkhäuser.
Rabin, M., Sue, C., Walpersdorf, A., Sakic, P., Albaric, J., & Fores, B. (2018). Present-day deformations of the Jura arc inferred by GPS surveying and earthquake focal mechanisms. *Tectonics, 37*, 3782–3804. https://doi.org/10.1029/2018TC005047
Radaideh, O. M. A., & Mosar, J. (2021). Cenozoic tectonic deformation along the Pontarlier strike-slip fault zone (Swiss and French Jura fold-and-thrust belt): Insights from paleostress and geomorphic analyses. *Tectonics*. https://doi.org/10.1029/2021TC006758
RA-RESIF. (1995). *RESIF-RAP French Accelerometric Network*. RESIF—Réseau Sismologique et géodésique Français.
Reinecker, J. Tingay, M., & Müller, B. (2003). Borehole breakout analysis from four-arm caliper logs. World Stress Map Project, 1–5
Reisdorf, A. G., Wetzel, A., Schlatter, R., & Jordan, P. (2011). The Staffelegg formation: A new stratigraphic scheme for the Early Jurassic of northern Switzerland. *Swiss Journal of Geosciences, 104*(1), 97–146. https://doi.org/10.1007/s00015-011-0057-1
Rime, V., Sommaruga, A., Schori, M., & Mosar, J. (2019). Tectonics of the Neuchâtel Jura Mountains: Insights from mapping and forward modelling. *Swiss Journal of Geosciences, 112*, 563–578. https://doi.org/10.1007/s00015-019-00349-y
Rollier, L. (1903). Le plissement de la chaine du Jura. *Annales De Géographie, 12*(66), 403–410. https://doi.org/10.3406/geo.1903.6377
Schaeren, G., & Norbert, J. (1989). Tunnels du Mont Terri et du Mont Russelin—La traversee des « roches a risques »: Marnes etmarnes a anhydrite. Juradurchquerungen—aktuelle Tunnelprojekte im Jura. *Mitteilungen Der Schweizerischen Gesellschaft Für Boden Und Felsmechanik, 119*, 19–24.
Schlunegger, F., Jordan, T. E., & Klaper, E. M. (1997). Controls of erosional denudation in the orogen on foreland basin evolution: The Oligocene central Swiss Molasse Basin as an example. *Tectonics, 16*, 823–840. https://doi.org/10.1029/97TC01657
Schumacher, M. E. (2002). Upper Rhine Graben: Role of preexisting structures during rift evolution. *Tectonics*. https://doi.org/10.1029/2001TC900022
Sibson, R. (1990). Rupture nucleation on unfavorably oriented faults. *Bulletin of the Seismological Society of America, 80*(6), 1580–1604.
Sick, B., Walter, M., & Joswig, M. (2012). Visual event screening of continuous seismic data by supersonograms. *Pure and Applied Geophysics*. https://doi.org/10.1007/s00024-012-0618-x
Singer, J., Diehl, T., Husen, S., Kissling, E., & Duretz, T. (2014). Alpine lithosphere slab rollback causing lower crustal seismicity in northern foreland. *Earth and Planetary Science Letters, 397*, 42–56. https://doi.org/10.1016/j.epsl.2014.04.002
Sommaruga, A. (1999). Decollement tectonics in the Jura foreland fold-and-thrust belt. *Marine and Petroleum Geology, 16*(2), 111–134. https://doi.org/10.1016/S0264-8172(98)00068-3
Sommaruga, A., & Burkhard, M. (1997). Seismic sections through the Alpine foreland—Jura Mountains. In O. A. Pfiffner, P. Lehner, P. Heitzmann, S. Müller, & A. Steck (Eds.), *Results of NRP 20—deep structure of the Swiss Alps* (pp. 45–53). Basel: Birkhäuser GmbH.
Sommaruga, A., Mosar, J., Schori, M., & Gruber, M. (2017). Chapter 20—the role of the triassic evaporites underneath the North Alpine Foreland. In J. I. Soto, J. F. Flinch, & G. Tari (Eds.), *Permo-Triassic Salt Provinces of Europe North Africa and the Atlantic Margins* (pp. 447–466). Elsevier. 10.1016/B978-0-12-809417-4.00021-5.
Sue, C., & Schmid, S. M. (2017). From ocean formation to mountain evolution in Alpine-type orogens. *Swiss Journal of Geosciences, 110*(2), 417–418. https://doi.org/10.1007/s00015-017-0273-4
Swisstopo. (2005). *Tektonische Karte der Schweiz 1.500,000*. Federal Office of Topography Swisstopo.
Thury, M., & Bossart, P. (1999). The Mont Terri rock laboratory, a new international research project in a Mesozoic shale formation, Switzerland. *Engineering Geology, 52*(3–4), 347–359. https://doi.org/10.1016/S0013-7952(99)00015-0
Ungerer, J. (1990). Berechnung von Nahfeldseismogrammen mit der Reflektivitatsmethode. Diploma Thesis, Institute of Geophysics, University of Stuttgart, Germany.
Ustaszewsi, K., Schuhmacher, M. E., & Schmid, S. M. (2005). Simultaneous normal faulting and extensional flexuring during rifting: An example from the southernmost Upper Rhine Graben. *International Journal of Earth Sciences, 94*, 680–696. https://doi.org/10.1007/s00531-004-0454-z
Ustaszewski, K., Schumacher, M. E., Schmid, S. M., & Nieuwland, D. (2005). Fault reactivation in brittle-viscous wrench systems—Dynamically scaled analogue models and application to the Rhine-Bresse Transfer Zone. *Quaternary Science Reviews, 24*, 363–380. https://doi.org/10.1016/j.quascirev.2004.03.015
Ustaszewski, K., & Schmid, S. M. (2006). Control of pre-existing faults on geometry and kinematics in the northernmost part of the Jura fold-and-thrust belt. *Tectonics*. https://doi.org/10.1029/2005TC001915
Ustaszewski, K., & Schmid, S. M. (2007). Latest Pliocene to recent thick-skinned tectonics at the Upper Rhine Graben—Jura Mountains junction. *Swiss Journal of Geosciences, 100*(2), 293–312. https://doi.org/10.1007/s00015-007-1226-0
Villiger, A., 2014. Improvement of the kinematic model of Switzerland (Swiss 4D II). Ph.D. Thesis, ETH Zürich. https://doi.org/10.3929/ethz-a-010163325.
Vouillamoz, N., Kraft, T., Abednego, M., & Diehl, T. (2016b). Lowering microseismic detection threshold in Northeastern Switzerland using sonogram analysis and template matching, Technical Report NAB 16–72, Nagra.
Vouillamoz, N., Mosar, J., & Deichmann, N. (2017). Multi-scale imaging of a slow active fault zone: Contribution for improved seismic hazard assessment in the Swiss Alpine foreland. *Swiss Journal of Geosciences, 110*(2), 547–563. https://doi.org/10.1007/s00015-017-0269-0
Vouillamoz, N., Wust-Bloch, G. H., Abednego, M., & Mosar, J. (2016). Optimizing Event Detection and Location in Low-Seismicity Zones: Case Study from Western Switzerland. *Bulletin of the Seismological Society of America, 106*(5), 2023–2036. https://doi.org/10.1785/0120160029
Waldhauser, F., & Ellsworth, W. L. (2000). A double-difference earthquake location algorithm: Method and application to the northern Hayward fault, California. *Bulletin of the Seismological Society of America, 90*(6), 1353–1368. https://doi.org/10.1785/0120000006
Weber, H. P., Sattel, G., & Sprecher, C. (1986). *Sondierbohrungen Weiach, Riniken, Schafisheim, Kaisten, Leuggern, Geophysikalische Daten, (Nagra Tech. Ber. NTB 85-50, Beilagenband)*. Nagra.
Wetzel, A., & Allia, V. (2003). Der Opalinuston in der Nordschweiz: Lithologie und Ablagerungsgeschichte. *Eclogae Geologicae Helvetiae, 96*, 451–469.
Wust-Bloch, G. H., & Joswig, M. (2006). Pre-collapse identification of sinkholes in unconsolidated media at Dead Sea area by 'nanoseismic monitoring' (graphical jackknife location of weak sources by few, low-SNR records). *Geophysical Journal International, 167*(3), 1220–1232. https://doi.org/10.1111/j.1365-246X.2006.03083.x
Ziegler, P. A. (1992). European Cenozoic rift system. *Tectonophysics, 208*, 91–111. https://doi.org/10.1016/0040-1951(92)90338-7
Ziegler, P. A., & Fraefel, M. (2009). Response of drainage systems to Neogene evolution of the Jura fold-and-thrust belt and Upper Rhine Graben. *Swiss Journal of Geoscience, 102*(1), 57–75. https://doi.org/10.1007/s00015-009-1306-4

Publisher's Note